Figure 1.

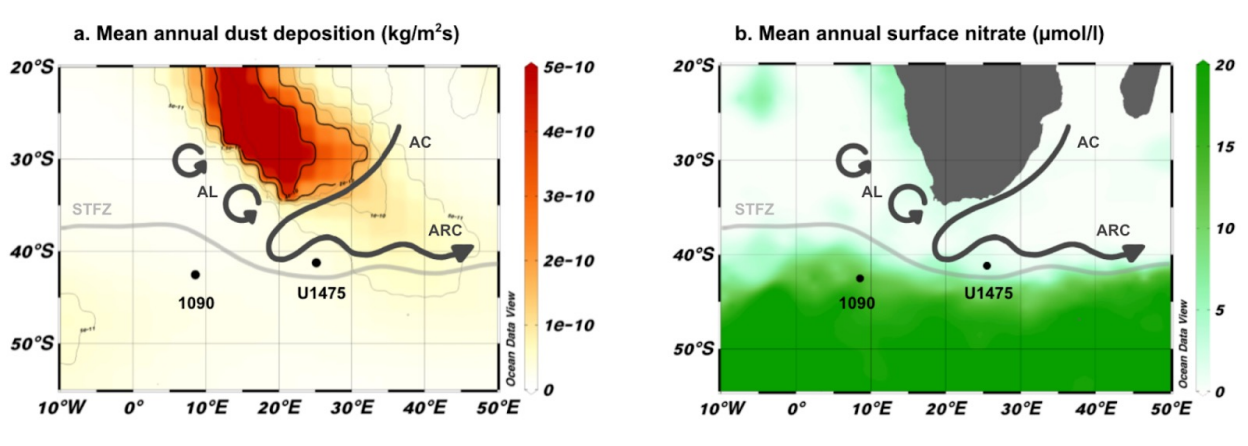
a. Mean annual dust deposition (kg/m²s)
20°S
30°S
40°S
50°S
10°W
0°
10°E
20°E
30°E
40°E
50°E
AC
AL
STFZ
ARC
1090
U1475
5e-10
4e-10
3e-10
2e-10
1e-10
0
Ocean Data View
b. Mean annual surface nitrate (µmol/l)
20°S
30°S
40°S
50°S
10°W
0°
10°E
20°E
30°E
40°E
50°E
AC
AL
STFZ
ARC
1090
U1475
20
15
10
5
0
Ocean Data View

Figure 2.

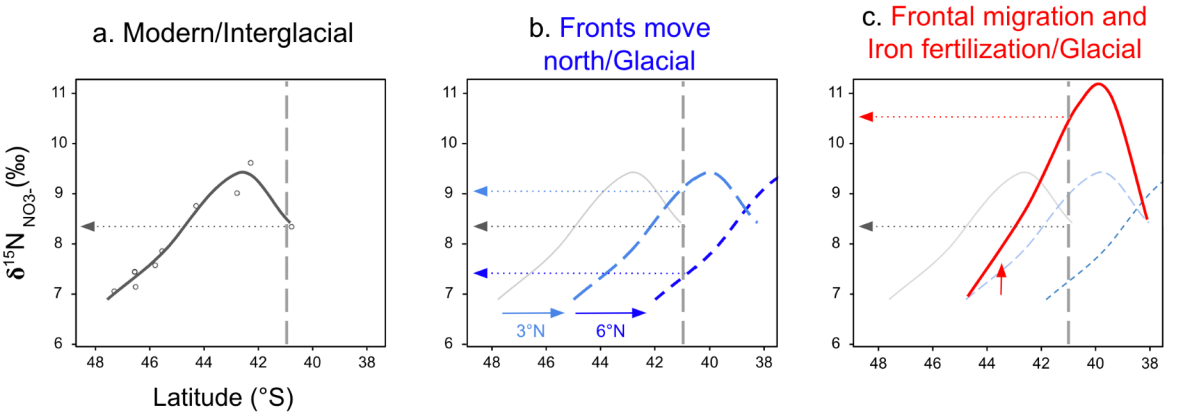
a. Modern/Interglacial
b. Fronts move north/Glacial
c. Frontal migration and Iron fertilization/Glacial
δ15NNO3- (‰)
Latitude (°S)
3°N
6°N
11
10
9
8
7
6
48
46
44
42
40
38

Figure 3.

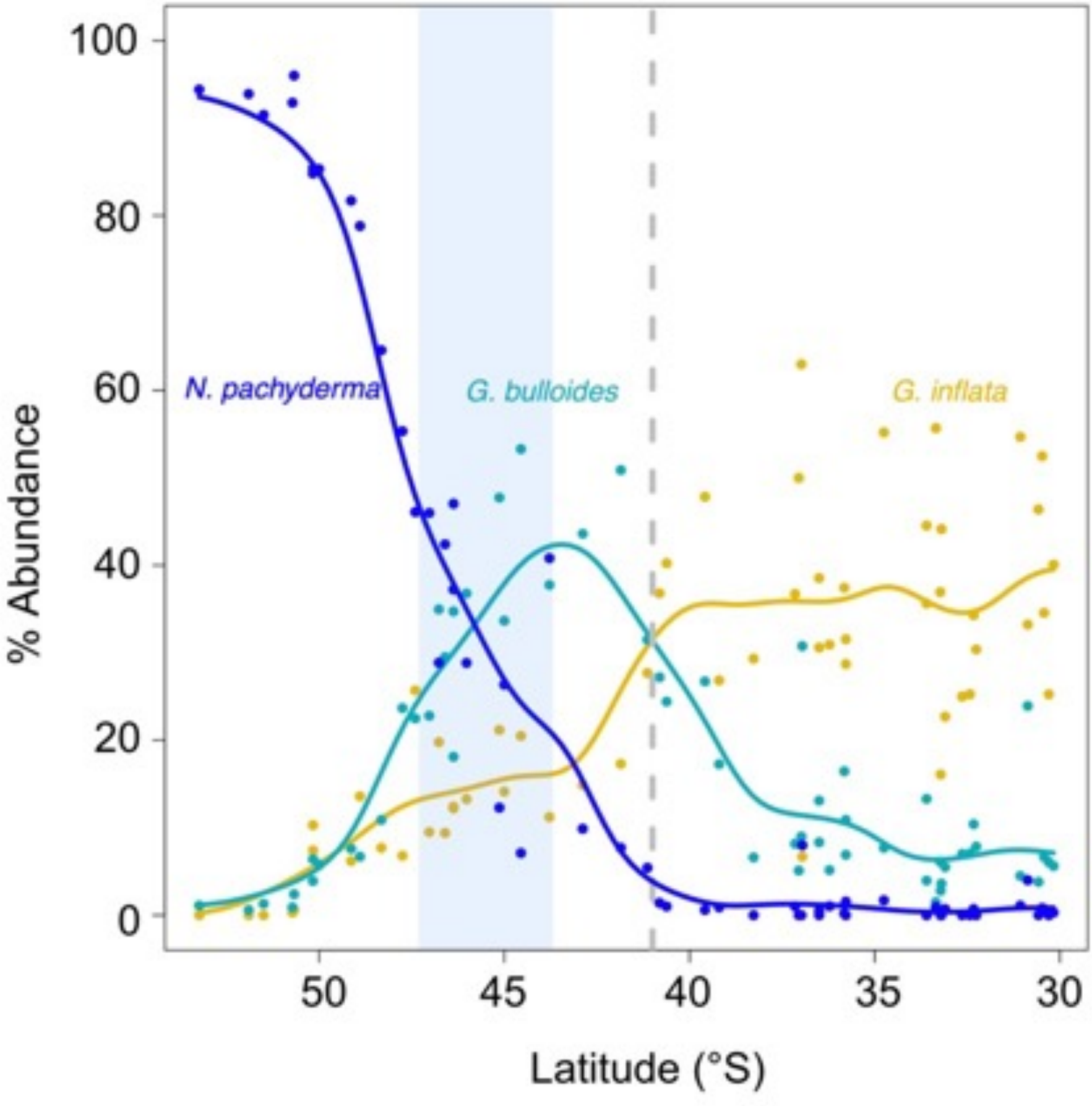
100
80
60
40
20
0
% Abundance
N. pachyderma
G. bulloides
G. inflata
50
45
40
35
30
Latitude (°S)

Figure 4.

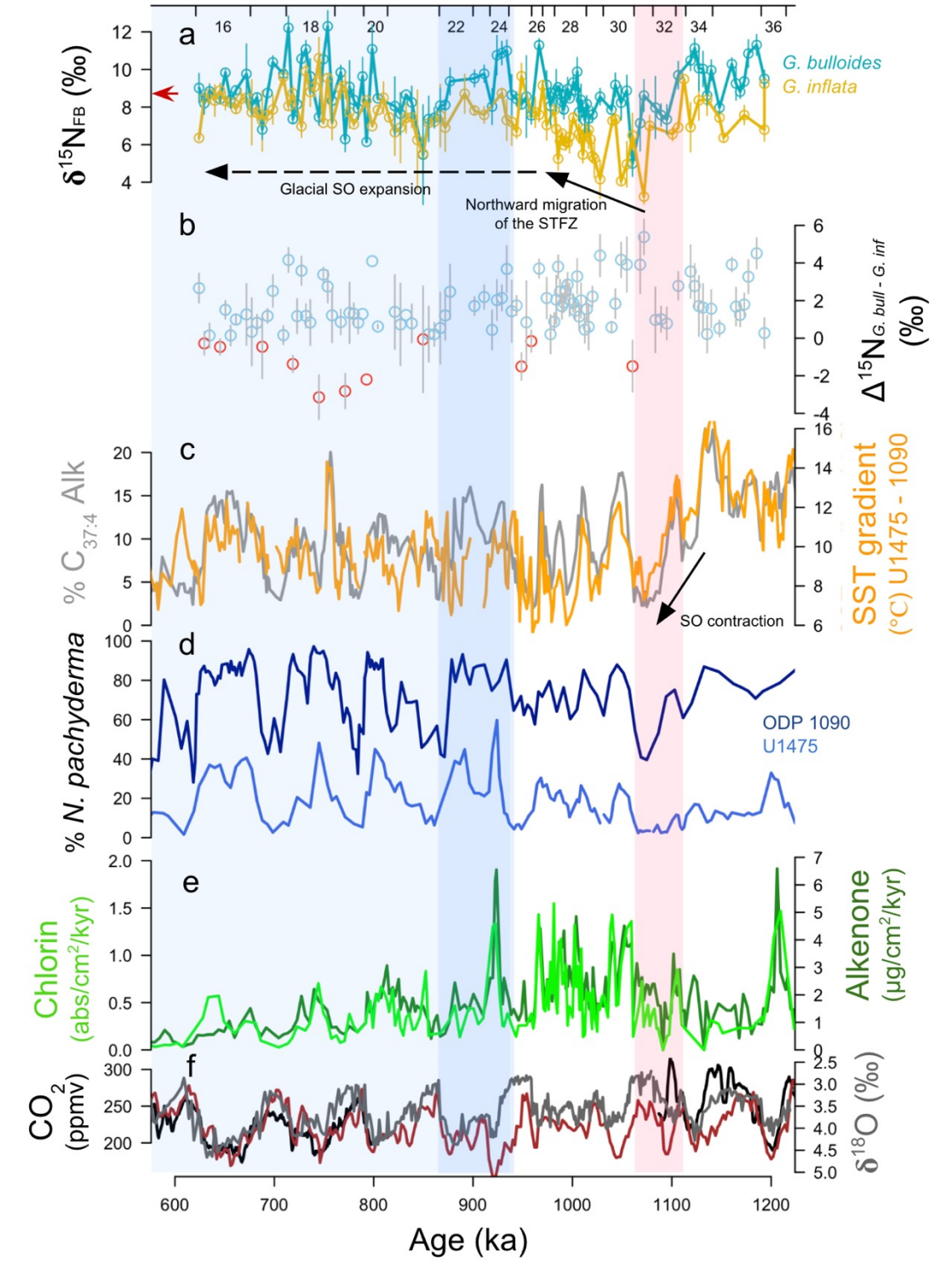
a
b
c
d
e
f
16
18
20
22
24
26
28
30
32
34
36
δ15NFB (‰)
G. bulloides
G. inflata
Glacial SO expansion
Northward migration of the STFZ
Δ15NG. bull - G. inf (‰)
% C37:4 Alk
SST gradient (°C) U1475 - 1090
SO contraction
% N. pachyderma
ODP 1090
U1475
Chlorin (abs/cm2/kyr)
Alkenone (µg/cm2/kyr)
CO2 (ppmv)
δ18O (‰)
600
700
800
900
1000
1100
1200
Age (ka)

Figure 5.

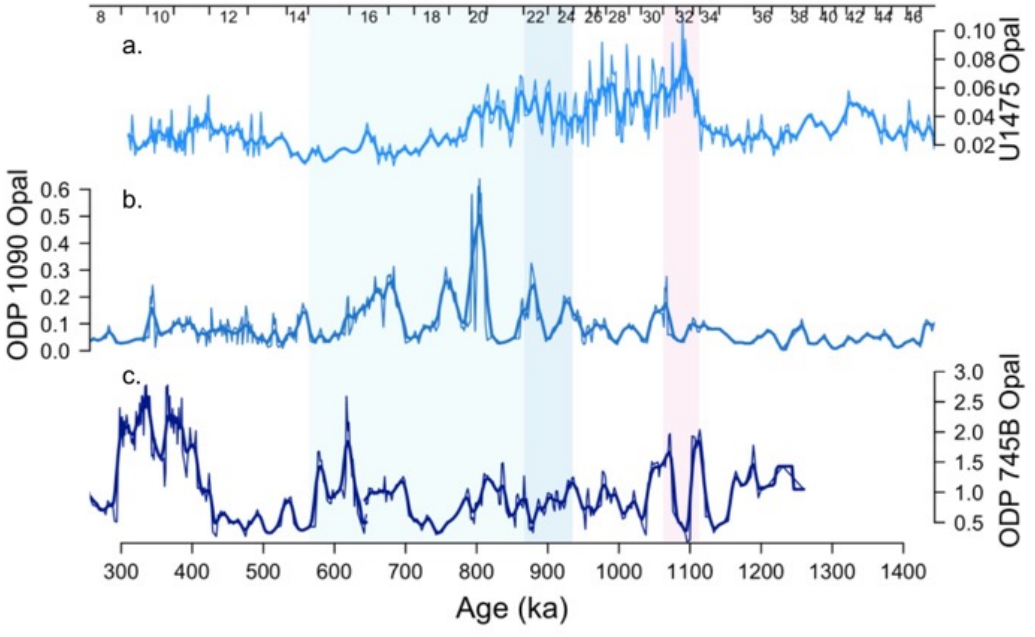
8
10
12
14
16
18
20
22
24
26
28
30
32
34
36
38
40
42
44
46
a.
0.10
0.08
0.06
0.04
0.02
U1475 Opal
b.
0.6
0.5
0.4
0.3
0.2
0.1
0.0
ODP 1090 Opal
c.
3.0
2.5
2.0
1.5
1.0
0.5
ODP 745B Opal
300
400
500
600
700
800
900
1000
1100
1200
1300
1400
Age (ka)

Figure 6.

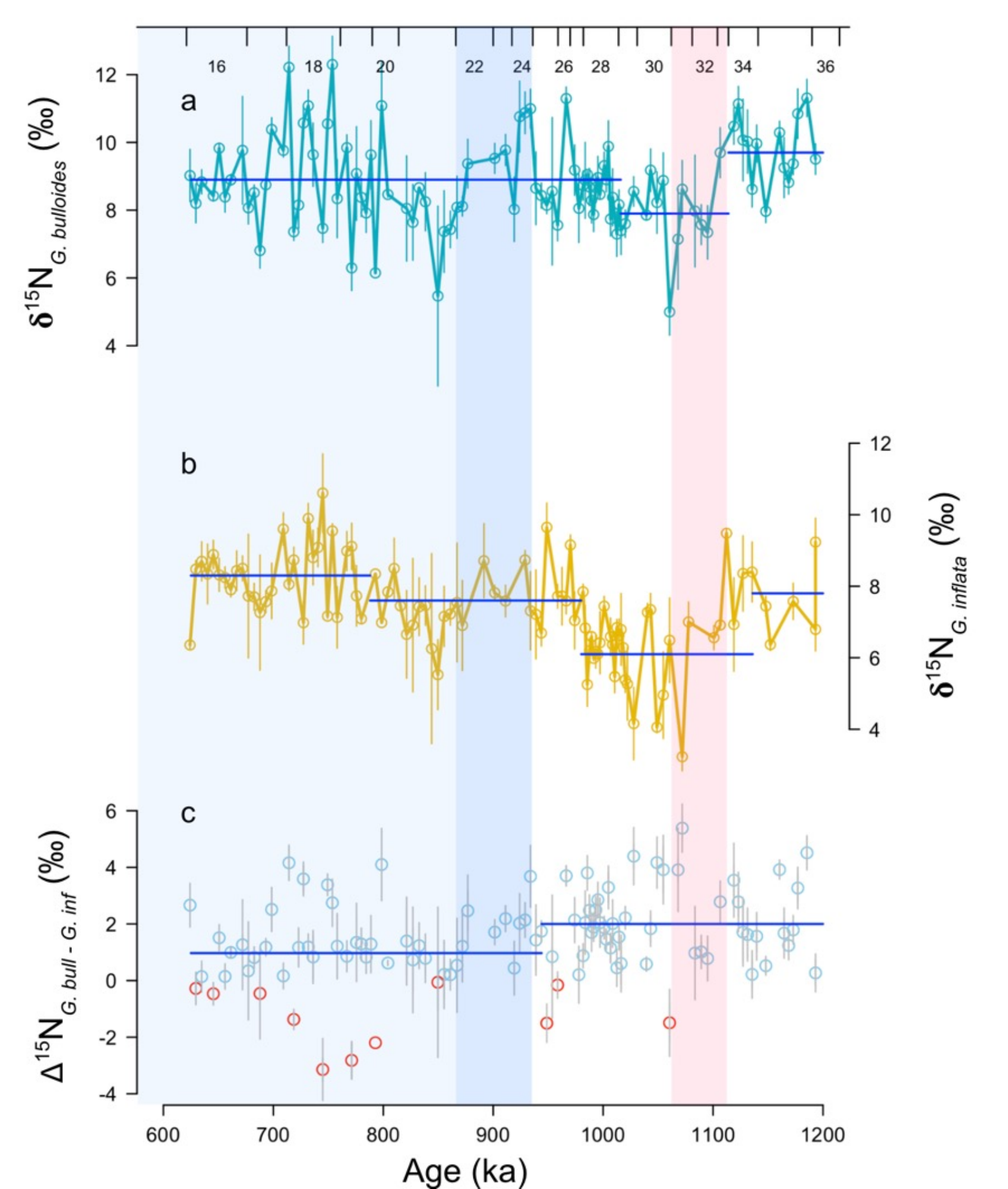
16
18
20
22
24
26
28
30
32
34
36
a
b
c
δ15N G. bulloides (‰)
δ15N G. inflata (‰)
Δ15N G. bull - G. inf (‰)
Age (ka)
600
700
800
900
1000
1100
1200

Glacial Southern Ocean expansion recorded in foraminifera-bound nitrogen isotopes from the Agulhas Plateau during the Mid-Pleistocene Transition

B. A. Marcks[1]*, T. P. Dos Santos[2], D. V. O. Lessa[2], A. Cartagena-Sierra[3], M. A. Berke[3], A. Starr[4], I. R. Hall[4], R. P. Kelly[1], R. S. Robinson[1]

[1]Graduate School of Oceanography, University of Rhode Island, Narragansett, RI, USA.
[2]Programa de Pós-Graduação em Geoquímica Ambiental, Universidade Federal Fluminense, Brazil.
[3]Department of Civil and Environmental Engineering and Earth Sciences, University of Notre Dame, Notre Dame, IN, USA.
[4]School of Earth and Environmental Sciences, Cardiff University, Cardiff, UK.
*Corresponding author: Basia Marcks (bmarcks@uri.edu)

Plain Language Summary:

The Mid-Pleistocene Transition is a unique period of time, during which the natural rhythm of Earth's climate shifted, the pace of glacial and interglacial cycles changed from 40,000 years to 100,000 years as ice sheets expanded, carbon accumulated in the deep ocean, and the planet cooled. The exact cause of these changes is unclear, but internal system feedbacks were likely at play. As climate changes today and the oceans increasingly take up carbon, the Mid-Pleistocene Transition provides a unique case study to investigate Earth's natural climate system and important carbon cycle feedbacks. In this paper we use the nitrogen isotopic composition of plankton shells and other biogeochemical records to show that leading up to the Mid-Pleistocene Transition the Southern Ocean underwent major physical changes and expanded as 100,000 year glacial cycles emerged. Our data indicates that the expansion of the Southern Ocean delivered cold, nutrient rich waters northward where they could mix with warm, salty Indian and Atlantic Ocean waters as hypothesized by other studies.

Key Points:

- Foraminifera-bound nitrogen isotope values from the Agulhas Plateau record latitudinal migrations of the Subtropical Front.
- Elevated foraminifera-bound nitrogen isotope values after 900 ka are consistent with Southern sourced nitrate.
- Southern Ocean contraction during a "super interglacial" brings more subtropical nitrate to the Agulhas Plateau.

Abstract

The emergence of 100-kyr glacial cycles (The Mid-Pleistocene Transition, MPT) is attributed in part to slower global overturning circulation and iron stimulation of biological carbon drawdown in the Southern Ocean. We present foraminifera-bound nitrogen isotope values and polar planktic foraminifera abundances from the Agulhas Plateau that show that increases in biogenic sediment accumulation coincide with northward migrations of the Subtropical Frontal Zone (STFZ) and elevated foraminifera-bound nitrogen isotope values during MPT glacial episodes. The nitrogen isotope values of two planktic foraminifera species, *Globigerina bulloides* and *Globorotalia inflata* show remarkable coherence amongst the sea surface temperature gradient between the STFZ and SAZ, and polar foraminifera abundances, indicating a strong relationship between nitrogen isotope dynamics above the Agulhas Plateau and migrations of the STFZ. Northward migration of the STFZ may have been essential to prolonging glacial intervals by increasing deep ocean carbon storage via a northward shift of the South Westerly Winds (SWW) and a reduction in upwelling, delivery of fresher surface waters into the upper limb of global overturning circulation, or inhibiting heat and salt delivery to the Atlantic as Agulhas Leakage.

1 Introduction

Around 1 million years ago (Ma), Antarctica and the Southern Ocean witnessed expansion of polar ice sheets and Southern Ocean sea ice (Starr et al., 2021) and increases in iron delivery and biological productivity in the Subantarctic Zone (SAZ) (Martínez-García et al., 2009; Kemp et al., 2010). Alongside evidence for increased deep ocean carbon storage (Farmer et al., 2019), these surface changes implicate a Southern Ocean driver in the extension and amplification of glacial-interglacial cycles from 40 kyr to ~100 kyr pacing during the MPT (1,200 - 600 ka) (Chalk et al., 2017; Hönisch et al., 2009; Pena & Goldstein, 2014; Lear et al., 2016; Hoogakker et al., 2006; Hasenfratz et al., 2019). Several hypotheses exist to explain the mechanisms responsible for the MPT. Enhanced biological pump efficiency, increasing carbon export from the surface (and atmosphere) to the deep ocean, as well as slower ocean circulation, reducing CO_2 outgassing and extending the residence time of carbon in the deep ocean, have been proposed. However, without evidence demonstrating an increase in Southern Ocean nutrient consumption, the relative importance of each process in reducing glacial atmospheric CO_2 across the MPT remains ambiguous (Martínez-García et al., 2009; Diekmann & Kuhn, 2002; Kemp et al., 2010; Jaccard et al., 2013; Crundwell et al., 2008). Observed increases in biogenic sediment accumulation in the glacial Southern Ocean SAZ across the MPT could result from iron fertilization or Southern Ocean expansion in response to cooling and Antarctic ice sheet growth (Martínez-García et al., 2009; Diekmann & Kuhn, 2002).

The evidence for the northward expansion of the Southern Ocean during the MPT comes from the Atlantic Sector of the Southern Ocean (Kemp et al., 2010; Diekmann & Kuhn, 2002) and more recently the Indian-Atlantic Ocean Gateway, south of Africa (Starr et al., 2021; Cartagena-Sierra et al., 2021; Tangunan et al., 2021). Expansion of the Southern Ocean via northward migrations of the STFZ and SWW slows global overturning circulation and increases deep ocean carbon storage (Russell et al., 206; Toggweiler et al., 2006; Marshall & Speer, 2012; Ferrari et al., 2014; Sigman et al., 2021). The Indian-Atlantic Ocean Gateway is globally significant due to the eddies of salty Indian Ocean surface waters that are shed into the Atlantic Ocean as Agulhas

Leakage (AL). AL contributes excess salt to the surface return flow of the Atlantic Meridional Overturning Circulation (AMOC) that is needed for deep convection and North Atlantic Deep Water (NADW) formation (Pena & Goldstein, 2014; Caley et al., 2012; Beal et al., 2011). Northward migrations of the STFZ have been proposed to cut off or limit AL on millennial and glacial interglacial timescales as well as during the MPT. Evidence for significantly reduced AL during intervals when the Antarctic Polar Front is thought to have moved at least 7 degrees northward comes from the South Atlantic (Bard and Rickaby, 2009; Kemp et al., 2010; Caley et al., 2012). Recent evidence for increased ice-rafted debris accumulation beneath the STFZ during the early stages of glacial periods across the MPT suggests an expansion of cool, fresh SAZ waters into the subtropics (Starr et al., 2021). This 'southern escape' of fresh water potentially increased the buoyancy of the surface return flow of the AMOC, reducing NADW formation, and slowing overturning (Starr et al., 2021; Pena & Goldstein, 2014). Whether by reducing salty AL or adding fresh water via the southern escape, these changes provide a physical means of carbon sequestration during the MPT (Starr et al., 2021; Simon et al., 2013). In this region, such dramatic northward migrations of the Southern Ocean fronts would also deliver excess macronutrients towards the subtropics, closer to South African and South American aeolian dust sources (Martin, 1990; Martínez-García et al., 2011; Martínez-García et al., 2014) (Figure 1). Given sufficient iron supply to Site U1475, the increase in nutrients would fuel local productivity further enhancing glacial carbon drawdown (Martin, 1990; Martínez-García et al., 2011; Martínez-García et al., 2014; Anderson et al., 2014). Indeed, northward STFZ migrations during glacial periods of the past 1.4 million years are met with increased productivity at Site U1475 with the most significant northward frontal migrations yielding the greatest increases in biogenic sediment deposition (Tangunan et al., 2021; Cartagena-Sierra et al., 2021).

While the MPT is widely regarded as an interval of global cooling, significant Southern Hemisphere warming occurs during the MPT "super interglacial", MIS 31, ~1,100 ka. Prior to the emergence of 100 kyr glacial-interglacial cyclicity, Southern Hemisphere insolation reaches a 5 Myr high, collapsing the East Antarctic Ice Sheet and delivering subtropical fauna well into the modern day Subantarctic Zone (Beltran et al., 2020; McKay et al., 2012; Maiorano et al., 2009). It is interesting that this destabilization of Antarctic ice sheets under relatively low atmospheric CO_2 concentrations occurs immediately prior to the re-equilibration of the global climate system with cooler and longer glacial intervals during the MPT. The role MIS 31 plays in the MPT remains ambiguous, highlighting the need for a greater understanding of how Southern Ocean processes influence and are influenced by global climate.

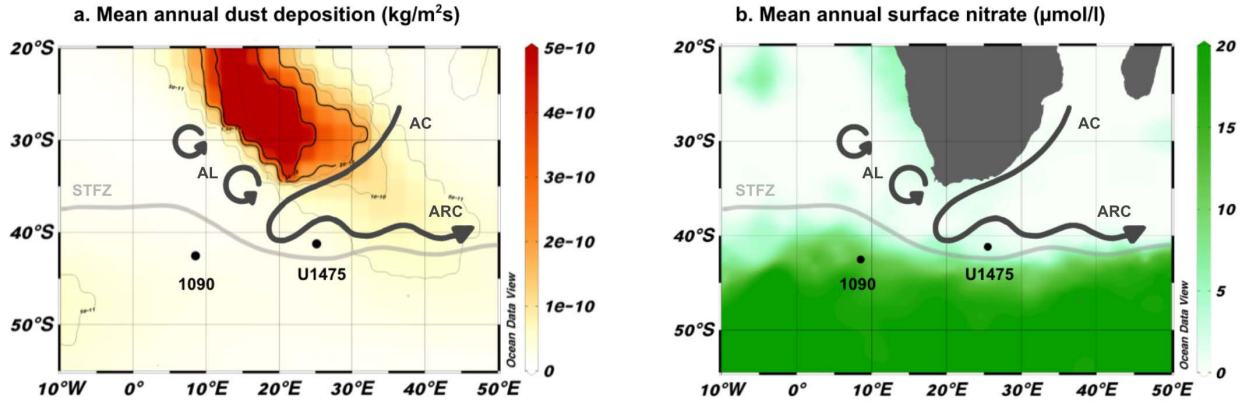

Figure 1: Map of Site U1475 and Site 1090, in the Indian-Atlantic Ocean gateway, with respect to modern a. mean annual dust deposition (kg/m^{2}s) (Li et al., 2008) and b. mean annual surface nitrate (µmol/l) (World Ocean Atlas, 2013). STFZ = Subtropical Frontal Zone; AL = Agulhas Leakage; AC = Agulhas Current; ARC = Agulhas Return Current. STFZ position from Orsi et al., (1995).

Here, we focus on the importance of frontal migrations as recorded in the nitrogen isotope values of foraminifera, in the Indian-Atlantic Ocean Gateway region across the MPT. Nitrogen isotopes provide us with a tool for documenting nutrient consumption within regions of the ocean where surface nitrate is not completely consumed and/or nutrient sources where nitrate is depleted. In the modern Southern Ocean, the nitrogen isotopic composition of nitrate, $\delta^{15}N_{NO3}$, where $\delta^{15}N = [(^{15}N/^{14}N)_{sample}/(^{15}N/^{14}N)_{air}] - 1$, increases with nutrient drawdown as surface waters are advected north, yielding maximum values at the northern edge of the Southern Ocean generally, and within in the STFZ south of Africa, specifically (Figure 2a; Smart et al., 2020; Ren et al., 2009; Sigman et al., 1999). In the oligotrophic subtropical Indian Ocean, near surface $\delta^{15}N_{NO3-}$ values tend to be lower than in the Southern Ocean surface, due in part to the addition of newly fixed nitrogen with a $\delta^{15}N$ of ~0‰ (Harms et al., 2019). The result is meridional increase in $\delta^{15}N_{NO3-}$ values across the Southern Ocean that peaks around 42-43°S, reflecting the progressive increase in nutrient consumption, and then a decrease beyond 42°S that reflects mixing of Southern Ocean sourced nitrate with subtropically sourced nitrate in the deep mixed layer of the STFZ (Figure 2a). This trend in the $\delta^{15}N_{NO3-}$ is reflected in the $\delta^{15}N$ of particulate organic nitrogen produced by phytoplankton using this nitrate pool and in turn, the particulate nitrogen is consumed by planktonic foraminifera and is the source of their $\delta^{15}N$ signal (Smart et al., 2020; Ren et al., 2009). We use the $\delta^{15}N$ values of organic matter within planktonic foraminifera shells ($\delta^{15}N_{FB}$) to study the surface nutrient dynamics in this mixing region, where the source of nitrate is the primary control on the $\delta^{15}N$ value of organic matter, yet the source $\delta^{15}N$ values are subject to change.

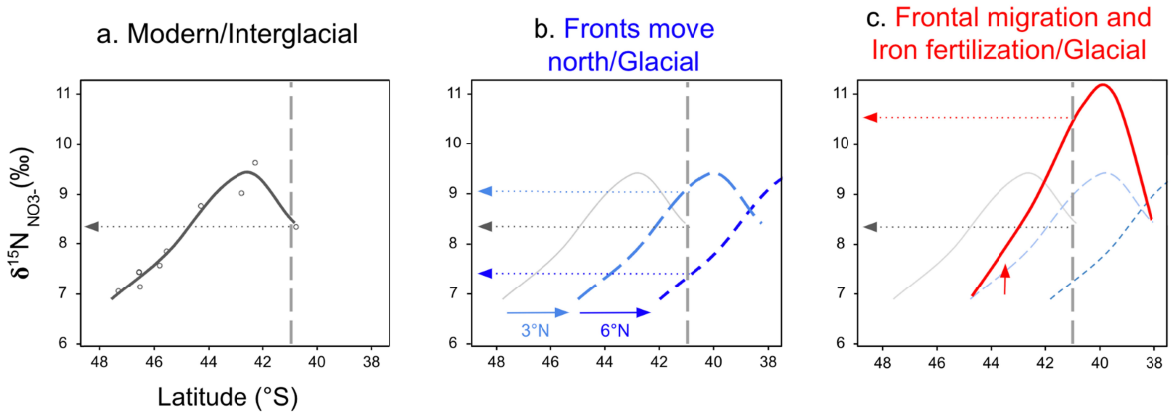

Figure 2: Schematic illustrating the $\delta^{15}N_{nitrate}$ latitudinal gradient in the modern ocean and estimated changes resulting from frontal migrations and/or iron fertilization. a. Modern $\delta^{15}N_{NO3-}$ latitudinal gradient within the Southern Ocean mixed layer (Smart et al., 2020); b. under hypothesized MPT scenarios of northward frontal migrations; c. and iron fertilization. Vertical dashed line approximates the location of Site U1475, within the present-day STFZ. Dotted arrows indicate expected $\delta^{15}N_{NO3-}$ at Site U1475 under each scenario.

To do so, we pair $\delta^{15}N_{FB}$ values with polar planktonic foraminifera species abundance, and sea surface temperatures (SST) from International Ocean Discovery Program Site U1475 (41°25′S, 25°15′E; water depth 2669 m) to provide constraints on the relative importance of physical (ocean circulation) and biological (export productivity) processes across the MPT. Site U1475 underlies the Subtropical Frontal Zone (STFZ) where warm, nutrient-poor subtropical waters meet cool, nutrient-rich polar waters at the northern edge of the Southern Ocean SAZ (Figure 1) thus it is sensitive to physical and biogeochemical changes associated with latitudinal migrations of the STFZ. We consider these additional physical water mass proxies in light of complimentary proxy records from ODP Site 1090 (42°54′S, 8°54′E; water depth 3702 m) which serves as an SAZ endmember.

We present records of $\delta^{15}N_{FB}$ from *Globigerina bulloides* ($\delta^{15}N_{FB\ G.\ bull}$) and *Globorotalia inflata* ($\delta^{15}N_{FB\ G.\ inf}$). *G. bulloides* is a cosmopolitan, opportunistic species inhabiting nutrient-rich environments, with maximum abundances south of the STFZ (Figure 3; Bé & Hutson, 1977; Haddam et al., 2016). *G. inflata* is dominant within the thermocline of transitional environments, between subtropical and polar water masses, with greatest abundance in the Indian Ocean north of Site U1475 (Figure 3; Bé & Hutson, 1977; Haddam et al., 2016). Previous studies measured $\delta^{15}N_{FB\ G.\ bull}$ to examine SAZ nutrient consumption at ODP 1090, located well within the SAZ. At U1475, within the STFZ, the $\delta^{15}N_{FB\ G.\ bull}$ may be biased toward a Southern Ocean signal and subject to potential influence from variations in SAZ nutrient demand related to Fe fertilization but also to the incursion of low latitude source nitrate into the mixing zone. $\delta^{15}N_{FB\ G.\ inf}$ values on the other hand, are more likely biased toward the Subtropical, or northern, component of the STFZ mixture. Comparison of the two records may relate to the relative position of the STFZ with respect to the core site.

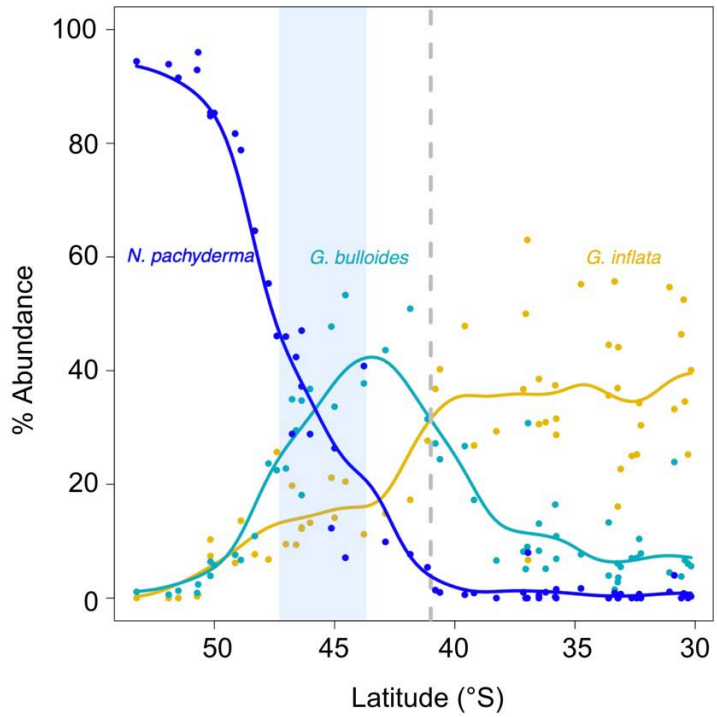

Figure 3: Modern core-top abundance of *N. pachyderma* sinistral (blue), *G. bulloides* (teal), *and G. inflata* (yellow) versus latitude in the region surrounding Site U1475, between 0 - 50 °E (Haddam et al., 2016). Blue shading encompasses latitudes in the modern ocean with abundances of *N. pachyderma* similar to observed glacial abundances during the MPT. Site U1475 denoted with grey dashed vertical line.

Our data demonstrate the northward migration of Southern Ocean fronts during MPT glacials. We show that the establishment of 100 kyr glacials is preceded by dramatic contraction of the Southern Ocean during the "super interglacial" Marine Isotope Stage 31, ~1,100 ka, and subsequent expansion of the Southern Ocean in the Indian-Atlantic Ocean Gateway. Expansion of the Southern Ocean appears to have occurred with an increase is biological carbon sequestration as due to enhanced biological pump efficiency in the Southern Ocean, while also altering global ocean circulation through mixing with Agulhas Leakage. Dilution of Agulhas Leakage by Southern Ocean waters may further heighten deep ocean carbon storage, increasing the residence time of surface waters and slowing overturning circulation (Starr et al., 2021).

2 Materials and Methods

2.1 Foraminifera-bound N isotopes

Individual species were identified and ~550 individuals per species were picked from the >250 µm fraction under dissecting microscope for each sample. Approximately 7 mg of picked and identified foraminifera shells were crushed between glass microscope slides and rinsed with MilliQ water. Samples were cleaned prior to $\delta^{15}N_{FB}$ measurement as follows: crushed tests were sonicated in 1.5 mL of 2% sodium hexametaphosphate, rinsed 5 times with MilliQ water and then chemically oxidized with 2 mL of an alkaline persulfate reagent (50 mL or MilliQ water, 3.25 g NaOH, 3.0 g $K_2S_2O_8$) in a pressure cooker for 60 minutes (~100 min with warm up and cool down) on a slow vent setting, followed by three MilliQ rinses, to remove external N

contamination (Smart et al., 2020; Ren et al., 2009). Once samples were clean, organic nitrogen was released into solution by acid dissolution of the foraminiferal calcite with 75 µL of 6N hydrochloric acid and converted to nitrate by the addition of 3 mL of an alkaline persulfate reagent (100 mL MilliQ water, 1.6 g NaOH, 1.0 g $K_2S_2O_8$; Knapp et al., 2005; Nydahl, 1978). Samples were acidified to a pH between 2-4, using ~100 µL 6N hydrochloric acid, prior to measurement. Nitrate concentrations were measured by chemiluminescence on a Teledyne Instruments (Model 200E) chemiluminescence NO/NOx analyzer (Braman & Hendrix, 1989). $\delta^{15}N_{FB}$ samples, 10 nmol in size, were measured by bacterial conversion of nitrate to nitrous oxide (Sigman et al., 2001), with measurement of the $\delta^{15}N$ of the nitrous oxide by automated extraction and gas chromatography-isotope ratio mass spectrometry (Casciotti et al., 2002) on a Thermo Delta V Plus IRMS. The potassium nitrate reference materials IAEA-N3 and USGS 34 (+4.7‰ and 1.8‰, respectively) were used to standardize results (Gonfiantini et al., 1995). Note, testing of subset of 6 samples, each with full procedural triplicates, for a total of 18 samples, showed negligible differences in nitrogen content and $\delta^{15}N_{FB}$ values with and without a reductive cleaning step, and so it was omitted here to avoid unnecessary loss of sample material.

Sample replicates and triplicates were analyzed when possible. Full procedural replicates were analyzed for 134 sample splits, representing 66 unique samples, when enough foraminifera were available for duplicate or triplicate analysis. The average standard deviation of procedural replicates is 0.4‰. Full operational blanks and amino acid standards (USGS 65 glycine) were measured in each batch. The average standard deviation of glycine standards measured in triplicate is 0.3‰. We estimated the $\delta^{15}N$ value of the persulfate blank using a dilution series (5, 7.5, 10, and 20 µM of the glycine standard and the fraction of the blank in standards. We applied a blank correction to each sample based on the calculated mean $\delta^{15}N$ value of all of the persulfate blanks for the dataset and the fraction of the blank in the N content of each sample (see SI equation S1). Data were subset to exclude N content outliers (>2 s.d. from mean and where the blank was greater than 20% of the sample N content, with significantly different $\delta^{15}N$ values from other replicates). The exclusion of this data does not alter statistical analyses or the findings of the paper but does improve error.

Full propagated analytical error associated with measurement and blank correction, following Higgins et al., (2009), was on average 0.6‰ (Full description in SI equation S2). Propagating the errors, including not only the procedural replicates and their variance, but the relative size of the blanks, the mean of the calculated blank $\delta^{15}N$ values (5± 10‰). All error bars are propagated errors for each individual sample where calculated and the mean value, 0.6‰, is used where procedural replicates were limited by sample availability. To verify accuracy, we measured the Holocene mean $\delta^{15}N_{FB\ G.\ bull}$ value at MD02-2588, a co-located CASQ core, of 8.7 ± 0.7‰; for comparison, $\delta^{15}N_{FB\ G.\ bull}$ value of the mudline sample collected at U1476 was measured to be 9.2 ‰ for *G. bulloides* size class 250-400 µm and 8.4‰ *bulloides* size class >400 µm (A. Foreman, personal communication, 2023. The age model is based on the benthic oxygen isotope stratigraphy presented by Starr et al. (2021). This age model for Site U1475 was generated with 12 radiocarbon dates and 33 benthic oxygen isotope tie points which were graphically aligned with a probabilistic stack of 180 globally distributed benthic oxygen isotope records (Starr et al., 2021).

2.2 Biogenic Silica

Approximately 200 mg of sediment was analyzed for each sample. Cleaning, chemical treatment, and measurement followed protocols outlined in (Mortlock & Froelich, 1989). Samples were measured with a UV Vis spectrophotometer at 812 nm wavelength. Full procedural replicates were performed on 163 of the 435 samples yielding an average standard deviation of 0.2%. Samples were referenced to RICCA VerSpec SiO_3^{2-} in 1% NaOH for intercomparison. Opal mass accumulation rates were calculated by multiplying the fraction of opal by dry bulk density and sedimentation rates from Starr et al. (2021).

2.3 Planktic foraminifera *Neogloboquadrina pachyderma* (sin) counts

Bulk planktonic foraminifera are obtained by washing ~ 10 cm^3 of sediment through a 150 μm sieve and drying at ~ 50 ºC for 24 h. This dried fraction is split until a total of 300-400 individuals remained. From this amount, we identify the relative abundance of *Neogloboquadrina pachyderma* tests according to Kennett and Srinivasan (1983) and Loeblich and Tappan (1988).

2.4 Changepoint mean analysis

Changepoint mean analysis was executed in R, using 'cpt.mean()' function within package 'changepoint' (RStudio Team, 2020) Data are averaged between replicates for each species and fit to a 6 kyr evenly spaced time series using nearest neighbor interpolation, R package 'pracma', function 'interp1().' Changepoint mean analysis was conducted using the following parameters: test statistic = Normal; method = PELT; penalty = BIC. We consider the 0.6‰ standard deviation in our interpretations, discussing short term changes greater than 1‰ and identifying long term changes in the mean. Welch 2-sample t tests on all samples and replicates analyzed in each section identified in the changepoint mean analysis show that each of the groups are significantly different ($p<0.05$) from each other.

3 Data

3.1 *Neogloboquadrina pachyderma* (sin) abundance

Relative abundance of *N. pachyderma* (sin) varies between glacial and interglacial intervals with greater abundances consistently observed in glacials. Prior to 936 ka, *N. pachyderma* (sin) generally increases from 0 – 10 % in interglacials to 20 – 30 % in glacials (Figure 4). From 936 – 917 ka, *N. pachyderma* (sin) dominates the assemblage, reaching 60 % abundance and remains above 20% throughout MIS 23 (917 – 900 ka, Figure 4). After 900 ka, *N. pachyderma* varies between 45% and 0% in glacial and interglacial intervals, respectively (Figure 4).

3.2 Opal mass accumulation

Opal concentrations were overall very low, with an average value of 1.6%, at U1475. As a result, opal mass accumulation rates are generally low (<0.05 mg/cm^2/kyr), reaching maximum values (> 0.1 mg/cm^2/kyr) early in the MPT, ~1,100 ka (Figure 5). After this initial peak, opal mass accumulation declines slightly, remaining near ~ 0.06 mg/cm^2/kyr until ~800 ka, after which opal accumulation remains largely below 0.05 mg/cm^2/kyr (Figure 5).

3.3 Foraminifera-bound N isotopes

Across the MPT, $\delta^{15}N_{FB\ G.\ bull}$ values are generally higher than $\delta^{15}N_{FB\ G.\ inf}$ values (Figure 4). While $\delta^{15}N_{FB\ G.\ bull}$ values are less variable and tend to be highest in the early MPT, prior to 1,100 ka, $\delta^{15}N_{FB\ G.\ inf}$ values are less variable and tend to be highest during the mid-late MPT, after ~790 ka. Both species exhibit minimum $\delta^{15}N_{FB}$ values during the "super interglacial" Marine Isotope Stage (MIS) 31, ~1,070 ka.

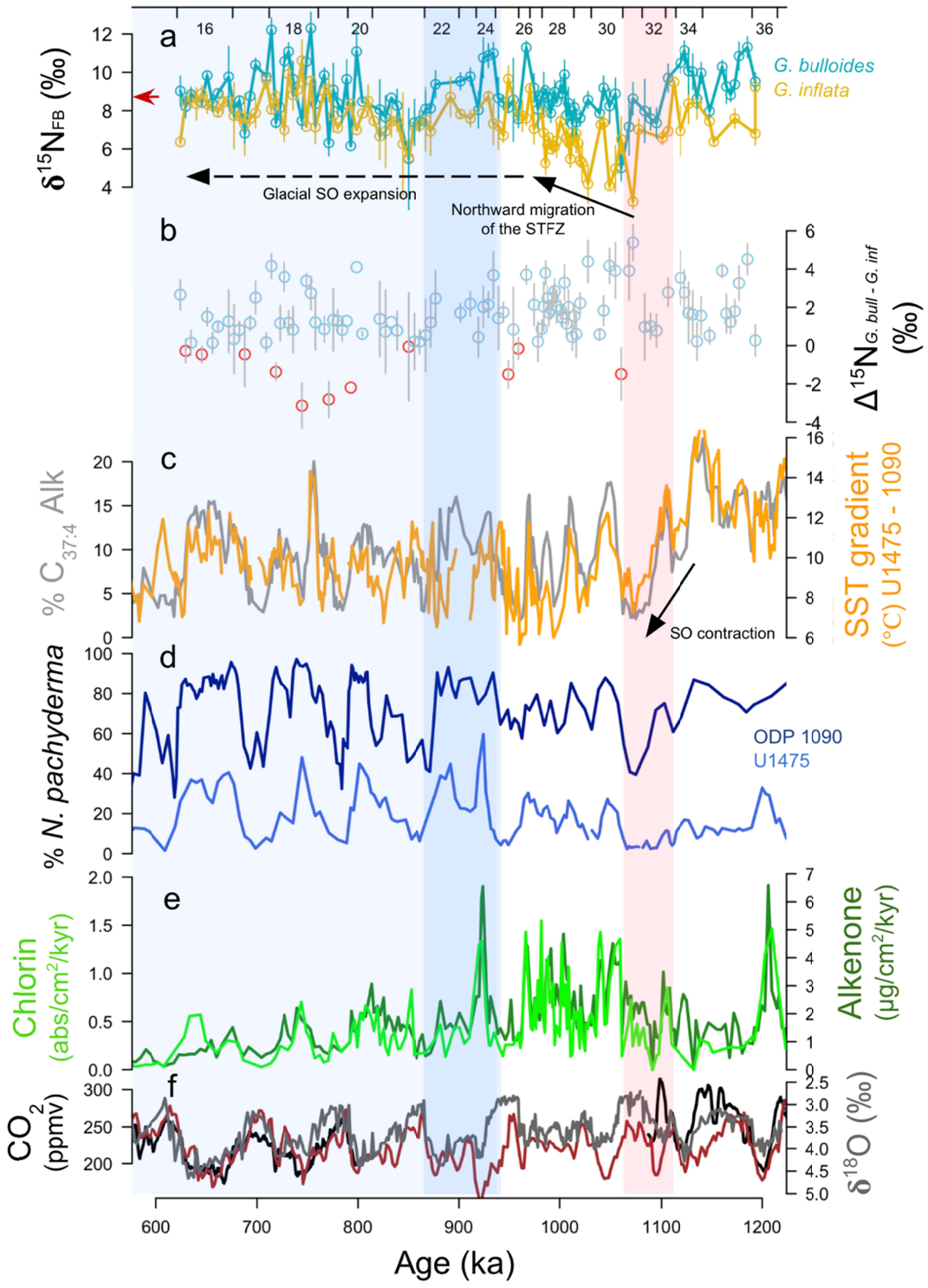

Figure 4: Biogeochemical records measured from Sites U1475 and ODP 1090. a. $\delta^{15}N_{FB}$ of *G. bulloides* and *G. Inflata*, vertical lines indicate propagated error for each sample. The average Holocene *G. bulloides* value from a co-located core (MD0202588) are indicated by the red arrow on the y axis; b. $\Delta\delta^{15}N_{FB}$, *G. bulloides – G. inflata*, where blue circles indicate positive and red indicate negative values, gray bars span vertical lines span ± 1 standard deviation; c. U^{k}_{37}' SST gradient between Site U1475 (Cartagena-Sierra et al., 2021) and ODP 1090 (Martínez-García et al., 2010) and percent $C_{37:4}$ alkenones at ODP 1090 (grey, Martínez-García et al., 2010); d. Percent abundance of

polar species *N. pachyderma* at Site U1475 and Site 1090 (Becquey & Gersonde, 2002); e. Alkenone and chlorin mass accumulation rates (Cartagena-Sierra et al., 2021) (μg/cm^2/kyr and abs/cm^2/kyr; dark and light green respectively). U1475 age model from Starr et al. (2021); f. Atmospheric CO_2 from EPICA Dome C (black, Bereiter et al., 2015), δ^{11}B-based reconstruction (black, Hönisch et al., 2009), and $\delta^{13}C_b$ models (red, Lisiecki, 2010); Site U1475 benthic δ^{18}O *Cibicidoides wuellerstorfi* (gray, Starr et al., 2021). Marine Isotope Stages are noted along the top axis. Light blue shading indicates 100 kyr world, dark blue shading indicates "900 kyr" event, red shading indicates "super interglacial".

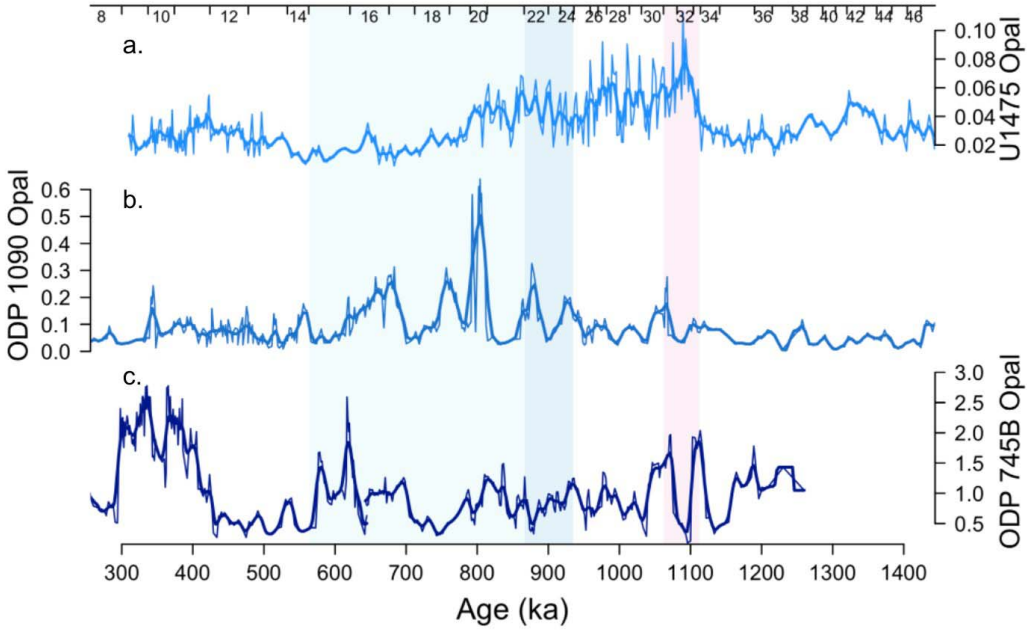

Figure 5: Opal mass accumulation rates (mg/cm^2/kyr) from the a. Subtropical frontal zone, IODP Site U1475; b. Subantarctic Zone, ODP Site 1090 (Diekmann & Kuhn, 2002); c. Antarctic Zone, ODP Site 745B (Kaiser et al., 2021; Billups et al., 2018) showing a southward shift in the relative, site specific, magnitude of biogenic opal deposition within the Southern Ocean around the MPT. Bold lines show a 10 kyr kernel smoothing. Marine Isotope Stages are noted along the top axis and red/blue shading corresponds to shading in Figure 4.

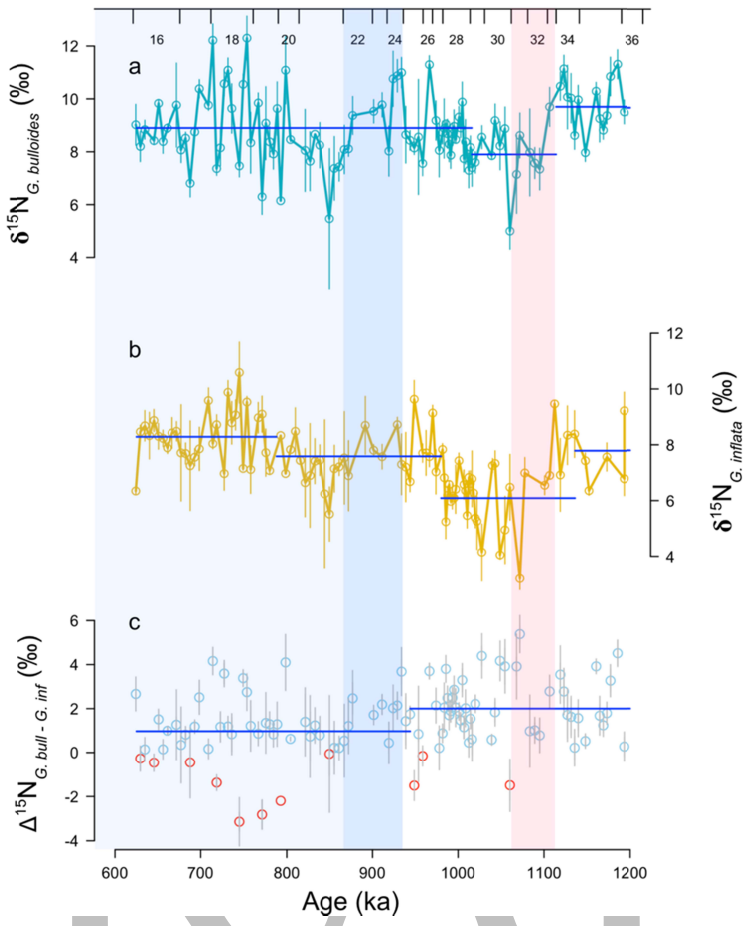

Figure 6: Results from changepoint mean analysis of a. $\delta^{15}N_{FB\ G.\ bulloides}$; b. $\delta^{15}N_{FB\ G.\ inflata}$; and c. $\Delta\delta^{15}N_{FB}$, *G. bulloides* – *G. inflata*, where blue circles indicate positive and red indicate negative values. Blue lines indicate mean $\delta^{15}N_{FB}$ of a statistically similar interval, with significant changes in the mean marked by a change in the y position, or mean $\delta^{15}N_{FB}$ value, of the line. Vertical bars span ± 1 standard deviation. Marine Isotope Stages are noted along the top axis and red/blue shading corresponds to shading in Figure 4.

4 Discussion

4.1 Long timescale changes in $\delta^{15}N$ above the Agulhas Plateau

The long timescale variation in $\delta^{15}N$, with lower $\delta^{15}N_{FB\ G.\ bull}$ and $\delta^{15}N_{FB\ G.\ inf}$ values around 1,100 ka, with a minimum during MIS 31-33, followed by a return to a more elevated mean values by 900ka, is mirrored in the SST gradient, $Uk'_{37:4}$, and *N. pachyderma* abundance records suggesting a strong link between surface ocean nutrient dynamics and the climate driven position of the Subtropical Front. Changepoint mean analysis reveals two significant timepoints in each species' $\delta^{15}N_{FB}$ record (Figure 6) that highlight the long term trends. From 1,200 – 1,114 ka the $\delta^{15}N_{FB\ G.\ bull}$ values vary around a mean of 9.7‰, a significant changepoint occurs at 1,114 ka when mean $\delta^{15}N_{FB\ G.\ bull}$ is reduced to 7.9‰ until 1,016 ka (Figure 6). After 1,016 ka $\delta^{15}N_{FB\ G.\ bull}$ values vary around a mean of ~ 8.9 ‰ (Figure 6). In contrast, $\delta^{15}N_{FB\ G.\ inf}$ values vary around a mean of 7.8‰ prior to 1,136 ka, from 1,136 – 980 ka mean $\delta^{15}N_{FB\ G.\ inf}$ is 6.1 ‰, from 980 – 788 ka mean $\delta^{15}N_{FB\ G.\ inf}$ is 7.6 ‰ and after 788 ka mean $\delta^{15}N_{FB\ G.\ inf}$ rises to 8.3 ‰ (Figure 6). The potential controls on the $\delta^{15}N$ records are: 1) variations in the relative contribution from

Subtropical versus Subpolar water masses, 2) variation in the relative contributions from locally grown versus advected foraminifera, 3) variations in the $\delta^{15}N$ values of the Subtropical source water, 4) variations in the $\delta^{15}N$ value of the Subpolar source, and 5) local variations in the relative utilization of nitrate. To some degree, all of these factors are likely to contribute to this record.

Subtropical and Subpolar waters converge in the STFZ and their relative contributions likely vary over time with climate. The early MPT, prior to ~1,140 ka, is marked by ice sheet expansion, cool SST's, and elevated *N. pachyderma* (sin) abundance at Site 1090 (McKay et al., 2012; Martínez-García et al., 2010; Beltran et al., 2020) (Figure 4; Figure S2). Yet, warm SST's and low *N. pachyderma* (sin) abundance at Site U1475 prior to 1,140 ka indicates the STFZ was located south of Site U1475. Records of Agulhas Leakage indicate transfer of water from the Indian into the Atlantic Ocean, consistent with this inference (Caley et al., 2012). The early MPT interval of ice-sheet expansion is terminated by the "super interglacial" of MIS 31 (~1,070 ka, McKay et al., 2012; Beltran et al., 2020) and a dramatic southward shift of the STFZ.

Southern Hemisphere insolation reaches a 5 Myr high during MIS 31, ~1,070 ka, resulting in dramatic Antarctic ice loss and Southern Hemisphere warming (Beltran et al., 2020; McKay et al., 2012; Maiorano et al., 2009) (Figure S2). Southward displacement of the STFZ is evidenced by reduced presence of polar species *N. pachyderma* (sin) at Site 1090, a sharp reduction in the SST gradient between Sites U1475 and 1090, reduced % $C_{37:4}$ at Site 1090 (Figure 4), and by increased presence of Subtropical Convergence/Agulhas Current nannofossil assemblages at Site 1090 from MIS 33-31 (1,114 – 1,062 ka, Maiorano et al., 2009). The reduced SST gradient is largely driven by warming at Site 1090 (Figure S2). This marks a sustained reduction in the SST gradient relative to values observed prior to MIS 33, ~1,110 ka (Figure 4). Interestingly, biogenic opal deposition at Site U1475 is highest during the "super interglacial", despite evidence for significant contraction of the Southern Ocean (Figure 5). The STFZ is associated with a deepening of the mixed layer depth and may indicate localized enhanced nutrient supply and consequent production related to this deep mixing (Monterey & Levitus, 1997).

The extreme southward shift in the STFZ is contemporaneous with significant reductions in the $\delta^{15}N_{FB}$ values. This interval is highlighted as a significant changepoint between MIS 33 – 31 (Figure 6). Low $\delta^{15}N_{FB}$ values are consistent with a greater contribution of nitrogen from the Subtropics, either through the advection of Subtropically sourced nitrate with low $\delta^{15}N$ values to the core site, resulting in low $\delta^{15}N$ PON production and consumption by local foraminifera, or the advection of more foraminifera from the Subtropics to the core site. Model results reveal the Agulhas Current is capable of carrying plankton nearly 1,000 km over a typical 30 day lifespan (van Sebille et al., 2015) and so at least some contribution from advected foraminifera is likely. While both potential contributions of nitrogen point to a more important Subtropical source during MIS 31 - 33, the need to make a distinction comes into play if one wants to assign an endmember $\delta^{15}N$ value to the Subtropical nitrogen or use the relative proportion of Subpolar versus subtropical planktic foraminiferal abundances to weight these endmember values. The possibility of locally grown versus imported foraminifera muddies these ideas further.

The need to understand the endmember $\delta^{15}N$ values is highlighted by the fact that the $\delta^{15}N_{FB}$ values observed during MIS 31-33 are exceptionally low relative to the rest of the record, and also relative to expectations based on to modern southern Indian Ocean values (Harms et al., 2016; Marshall et al., 2023). These low $\delta^{15}N_{FB}$ values require not only an increase in contributions of Subtropical nitrogen but also a decrease in the $\delta^{15}N$ of the nitrogen sourced to the STFZ. A decrease in the $\delta^{15}N$ of the Subtropically sourced nitrogen can be explained by increases in nitrogen fixation derived nitrogen in the Agulhas Current region. Today N fixation, which brings in N with a $\delta^{15}N$ value of ~-1‰, occurs in the source regions to and along the flowpath of the Agulhas Current (Dupuy et al., 2016; Kolasinski et al., 2012; Marshall et al., 2023). In addition, throughout interglacial periods of the last 800 kyr, increased denitrification has been documented in the Arabian Sea (Kim et al., 2018) thus it is probable that during this "super interglacial" we may see an exceptional response in N fixation to balance N losses from denitrification. Our data pose an interesting question as to whether a significant change in the magnitude of Indian Ocean denitrification and N fixation occurs at this time. N isotope data from upstream locations would be useful in confirming these changes.

At the same time that Subpolar nitrate likely became less important at U1475, the $\delta^{15}N$ of the Subpolar sourced nitrogen, either as nitrate or in advected Subpolar foraminifera, may also have decreased. Prior to the super-interglacial warming, we observe high $\delta^{15}N_{FB}$ values particularly in *G. bulloides* coincident with the SST gradient and Site 1090 $\%C_{37:4}$ maxima and Southern Hemisphere insolation minimum (Figure 4, Figure S2). Part of the elevation in $\delta^{15}N$ values may be due to the northward shifted Southern Ocean fronts, documented by the Site 1090 *N. pachyderma* (sin) and SST gradient data, and the associated relative contribution of Subpolar nitrogen at U1475. Yet, the observed $\delta^{15}N_{FB\ G.\ bull}$ values (11‰) exceed the modern latitudinal $\delta^{15}N_{NO3-}$ maxima expected near the STFZ (9.5‰) and are ~3‰ greater than the expected $\delta^{15}N_{FB\ G.\ bull}$ (Figure S1). This implies an increase in the $\delta^{15}N$ value of the source nitrogen. We infer that relative nutrient consumption was elevating the $\delta^{15}N$ value of nitrate (Figure 1, Figure 4). This could be due to a local increase in nutrient consumption or a regional increase and the advection of this signal northwards from the SAZ. Without an increase in productivity at Sites 1090 or U1475, enhanced nutrient consumption requires an overall reduction in nutrient supply prior to 1,110 ka. Indeed, ice sheet expansion may have contributed to weaker overturning within the Southern Ocean that limited nutrient supply and increased relative nitrate consumption regionally (Starr et al., 2021; Ferrari et al., 2014). After 1,110 ka, Southern Ocean warming during "super interglacial" MIS 31 coincides with a significant reduction in $\delta^{15}N_{FB}$ values and a decrease in the $\delta^{15}N$ of nitrogen from both the Subtropical and Subpolar sources is likely.

4.3 Transitional expansion of the glacial Southern Ocean prior to the 100 kyr glacial periods

The Southern Ocean experienced significant geographic expansion during glacial stages following 900 ka. *N. pachyderma* (sin) abundances indicate that the glacial expansions began gradually after MIS 31, (~1,060 ka), increasing in each glacial period until MIS 24 (~930 ka) when the STFZ achieved its northernmost position. At ~930 ka, *N. pachyderma* (sin) abundances exceeded 60% at Site U1475, which, based on *N. pachyderma* (sin) surface sediment distributions suggest an 8 degree northward migration in the average latitude of STFZ (Figures 3 & 4). Higher abundances of *N. pachyderma* (sin) in 100 kyr glacials, after ~920 ka, indicates increased influence of polar waters near Site U1475. The northward shift in polar waters is

supported by the relative proportion of the cold, $\%C_{37:4}$ alkenones at the nearby SAZ ODP Site 1090 (Martínez-García et al., 2010) (Figure 4) and abundance of ice-rafted debris (IRD) at Site U1475 (Figure S2, Starr et al., 2021). This northward migration of the STFZ would deliver nitrate rich waters further north, fueling the enhanced export productivity recorded by chlorin and alkenone accumulation from ~1,010 – 920 ka (Figure 4). The relatively high $\delta^{15}N$ of this southern sourced nitrate is evident in the progressive increase in $\delta^{15}N_{FB}$ values (Figure 6).

4.4 An expanded glacial Southern Ocean amplifies Fe fertilization in the 100 kyr world

The $\delta^{15}N_{FB}$ values at Site U1475 after 900 ka likely reflect the increased or dominant presence of the Southern Ocean waters that, because they are nutrient bearing, also record the nutrient consumption signal attributable to enhanced iron delivery (Martinez-Garcia et al., 2011). The STFZ maintains a northward position, as evidenced by *N. pachyderma* (sin) abundance and IRD deposition, from ~930 – 860 ka and, based on the relatively high $\delta^{15}N_{FB}$ values, an extended period of enhanced nutrient drawdown (Figure 4, Figure S2). Similar to the interval prior to the super-interglacial, expansion of the Southern Ocean alone cannot fully explain the glacial $\delta^{15}N_{FB}$ values recorded at Site U1475. A slowdown in overturning circulation is recorded by the accumulation of respired organic carbon in the deep ocean (Farmer et al., 2017; Lear et al., 2016). Expanded Southern Ocean sea ice and enhanced stratification at ~900 ka would have limited the supply of nutrients and carbon to the surface contributing to the elevated $\delta^{15}N_{FB}$ values observed across this interval (Hasenfratz et al., 2019). This interplay between biological drawdown and physical trapping of carbon occurs across the "900 ka event", prior to the establishment of 100 kyr cyclicity in deep ocean biogeochemical records (Ford & Chalk; 2020; Starr et al., 2021; Farmer et al., 2019; Pena & Goldstein, 2014).

In glacial intervals following 900 ka, the supply of southern sourced nutrients to Site U1475 supported modest increases in biological productivity that are reflected in slightly elevated biogenic sediment accumulation rates while elevated glacial $\delta^{15}N_{FB}$ values suggest continued greater demand for nutrients and reduced Subtropical nitrogen contributions (Figure S3). The expectation for a slight northward shift in the fronts without any change in the degree of nutrient consumption regionally is an increase in the $\delta^{15}N_{NO3-}$ value (due to reduced contribution of low $\delta^{15}N$ subtropical NO_3^-). While a larger northward shift in the latitude of the STFZ, as predicted in MPT glacials by *N. pachyderma* (sin) abundances (Figure 2b), would result in lower $\delta^{15}N_{NO3-}$, unless a significant increase in nutrient demand relative to availability accompanies these frontal migrations. Glacial *N. pachyderma* (sin) abundances indicate a 3 - 6 degree northward migration of the STFZ, again suggesting that the $\delta^{15}N_{FB}$ enrichments, on average 3‰ between average interglacial minima and glacial maxima cannot be explained without enhanced nutrient consumption (Figure 2 & 4) (Haddam et al., 2016). We use $\delta^{15}N_{FB\ G.\ bull}$ values to estimate a change in Southern Ocean nutrient consumption on glacial-interglacial timescales during the MPT, assuming the $\delta^{15}N_{FB\ G.\ bull}$ signal after MIS 31 dominantly reflects changes in relative consumption. We use measurements from *G. bulloides* to more easily relate to estimates from Site 1090 spanning the last glacial period.

Assuming no net change in supplied nitrate concentration or isotopic composition at 41°S, we apply a Rayleigh model to estimate changes in the degree of summer nitrate consumption associated with a 3‰ increase in $\delta^{15}N_{FB\ G.\ bull}$ (Altabet & Francois, 1994; Fripiat et al., 2019)

(Figure S1b). We calculate the integrated phytoplankton biomass N assimilated during summer nitrate drawdown using the "integrated product" equation, where $\delta^{15}N_{integ.prod.} = \delta^{15}N_{initial} + e * ([NO_3\text{-}]/([NO_3\text{-}]_{initial} - [NO_3\text{-}])) * \ln([NO_3]/[NO_3^-]_{initial})$ and $[NO_3^-]_{initial}$ and $\delta^{15}N_{initial}$ are the nitrate concentration and $\delta^{15}N_{NO3-}$ in the water supplied to the summertime surface mixed layer prior to nutrient drawdown, $[NO_3^-]$ is the nitrate concentration after the nutrient drawdown period, and e is the isotope effect of nitrate assimilation. Here we assume an isotope effect of 6.5‰, consistent with estimates for SAZ surface layer nitrate drawdown (DiFiore et al., 2010) (Figure S1). $\delta^{15}N_{initial}$ and $[NO_3^-]_{initial}$ are taken from water column measurements beneath the mixed layer at 41°S, 10.1‰ and 8.4 µM (Smart et al., 2020). Using these parameters, the $\delta^{15}N$ of the photosynthetic biomass produced is estimated to be 4.4‰, and $\delta^{15}N_{FB\ G.\ bull}$ is expected to be 7.5‰, based on a 3.1‰ trophic offset (Smart et al., 2020) (Figure S1b). These estimates are slightly lower than average interglacial data (8.7‰) and Holocene data (8.7‰) from Site U1475. Assuming similar conditions to modern, we use the integrated product estimation to link changes in $\delta^{15}N_{FB}$ values to nitrate consumption. Under these conditions, mean glacial maxima $\delta^{15}N_{FB}$ values of 10.2‰ and MIS 24 values of 10‰ are consistent with surface ocean nitrate concentrations below 2.2 µM (Figure S1b). Surface ocean nitrate concentrations indicate near complete nutrient consumption in glacial intervals with potentially >70% of surface ocean nutrients at Site U1475 drawn down. Between peak interglacial and glacial conditions, we estimate that relative nutrient consumption increased from 16% up to 70%, consistent with nutrient drawdown exceeding the increase in nutrient supply (Figure 4; Figure S1b). This estimate does not reflect the real nuances discussed above associated with the potential variations in the source $\delta^{15}N$ values or relative contributions of advected versus locally grown foraminifera.

If glacial mixing of SAZ and subtropical water remains similar amongst glacial periods following 900 ka, as the consistent glacial abundances of *N. pachyderma* (sin) imply, maintaining similar mean $\delta^{15}N_{FB}$ values with smaller magnitude increases in biogenic sediment accumulation requires that nutrient supply decreased. This can be explained by a wholesale slowdown in nutrient supply or a shift in the locus of nutrient consumption and the advection of the nitrogen isotopic signature of enhanced consumption northwards. Intermittent increases in biogenic opal accumulation occur in the SAZ after 900 ka and after 400 ka in the AZ perhaps suggesting a progressive southward shift in productivity (Figure 5) (Diekmann & Kuhn, 2002; Billups et al., 2018; Kaiser et al., 2021). Our observation supports a more polar Southern Ocean driver, whether biological or physical, of carbon sequestration during late MPT glacials.

Species specific differences in $\delta^{15}N_{FB}$

In addition to the large scale shifts in the mean $\delta^{15}N_{FB}$ seen in both the *G. bulloides* and *G. inflata* datasets, differences between the two records and the differences between species also vary with the inferred latitudinal migrations of the STFZ (Figure 6). A significant changepoint occurs in the record of the $\delta^{15}N_{FB}$ difference between the species ($\Delta\delta^{15}N_{FB} = \delta^{15}N_{FB\ G.\ bull} - \delta^{15}N_{FB\ G.\ inf}$), with decrease in the $\Delta\delta^{15}N_{FB}$ across the MPT with a >1 ‰ reduction in the mean after 933 ka reducing $\Delta\delta^{15}N_{FB}$ value from ~ 2.5 ‰ to 1.1 ‰ (Figure 6). The consistent offset between $\delta^{15}N_{FB\ G.\ bull}$ and $\delta^{15}N_{FB\ G.\ inf}$ values, in which $\delta^{15}N_{FB\ G.\ bull}$ values are higher, is counter to modern observations collected from net tows and sediment traps in Indian-Atlantic Ocean Gateway (Smart et al., 2020) (Figures 4 & 6). In the modern ocean, *G. inflata* records a higher

$\delta^{15}N_{FB}$ value than *G. bulloides* captured in the same net tow. This is attributable to its preference for a deeper habitat, possibly related to the consumption of a more degraded PON pool for nutrition (Smart et al., 2020). If depth was the primary control on differences between $\delta^{15}N_{FB\ G.\ bull}$ and $\delta^{15}N_{FB\ G.\ inf}$ values in the Site U1475 record we would expect to see consistently higher $\delta^{15}N_{FB\ G.\ inf}$ values. Since we do not, we explore the possibility that the differences relate to seasonal export events and/or foraminiferal habitat preferences and advection.

Within the Southern Ocean, *G. bulloides* exhibits two export episodes to the sediments each year, once in spring and again in fall (Kretschmer et al., 2018; King & Howard, 2005; Jonkers & Kučera, 2015). In contrast, *G. inflata* export flux peaks once, in spring (Jonkers & Kučera, 2015; Bé & Hutson, 1977). Thus, seasonal biases may yield higher $\delta^{15}N_{FB}$ values in *G. bulloides* if nutrients are more depleted in fall than in spring. This is not entirely consistent with modern observations from this region where late summer $\delta^{15}N_{NO3-}$ values are reduced by mixing with low $\delta^{15}N_{NO3-}$ subtropical waters indicating that seasonality does not provide a robust explanation (Smart et al., 2020). Further, as climate cools *G. bulloides* is expected to bias its export towards warmer seasons while *G. inflata* would be less affected; this could further reduce the $\delta^{15}N_{FB\ G.\ bull}$ relative to $\delta^{15}N_{FB\ G.\ inf}$ (Jonkers & Kučera, 2015).

However, planktic foraminifera are also subject to advection into this mixing zone. North of Site U1475, *G. inflata* is present in greater abundance than *G. bulloides*, but to the south *G. bulloides* abundance exceeds *G. inflata* (Figure 2). If we view the STFZ as a convergence zone of subtropical and subpolar planktic foraminifera, we can explain the observed $\delta^{15}N_{FB}$ values of *G. bulloides* and *G. inflata* more easily. On average, the *G. inflata* measured at Site U1475 are biased towards recording the subtropical signature of the Agulhas Current, where at least some fraction of the *G. inflata* in the sediment must have integrated the low $\delta^{15}N$ PON signal into their shell in the Subtropics to be ultimately deposited along the STFZ. Similarly, Ekman transport of Southern Ocean surface water would deliver *G. bulloides* grown in the SAZ to Site U1475. Some contribution of advected *G. bulloides* from the south and *G. inflata* from the north best explains the higher $\delta^{15}N$ values of *G. bulloides* compared to *G. inflata.* The difference between $\delta^{15}N_{FB}$ values of *G. bulloides* and *G. inflata* is smallest during "super interglacial" MIS 31 and after 933 ka, with the most similar values occurring when *N. pachyderma* (sin) abundances indicate considerable latitudinal migrations of the STFZ leading to greater similarity in $\delta^{15}N$ values of the sources to both species (Figure 4). To put it another way, when the front is furthest from U1475, either to the north or south, foraminifera $\delta^{15}N$ values reflect a shared local Subantarctic or Subtropical food source, whereas when the mixing zone is close to overhead, foraminifera are advected from different regions.

Both species exhibit significant changes in their mean $\delta^{15}N_{FB}$ values associated with these significant frontal migrations, however, *G. inflata*'s changes lag relative to *G. bulloides*, suggesting that $\delta^{15}N_{FB\ G.\ bull}$ is a sensitive and early indicator of southward migrations of the STFZ, with reductions in $\delta^{15}N_{FB\ G.\ bull}$ occurring as early as MIS 33 (Figure 6). After MIS 31, the $\delta^{15}N_{FB}$ values of both species significantly increase (Figure 6). The earlier increase in mean values of *G. bulloides* is consistent with a northward migration of the STFZ and expansion of the southern sourced $\delta^{15}N$ signal (Figure 6).

5 Conclusions

Across the MPT, $\delta^{15}N_{FB}$ records from Site U1475 change in tandem with STFZ migrations. The largest change in $\delta^{15}N_{FB}$ values results from Southern Ocean contraction and dominance of a low $\delta^{15}N$ subtropical nutrient signal during the "super interglacial" MIS 31, ~1080 ka. Glacial intervals prior to MIS 31 were cold in the Subantarctic but still relatively warm in the STFZ with the front located firmly south of the Agulhas Plateau. Glacials following MIS 31 are characterized by northward migrations of the STFZ in the Indian-Atlantic Ocean Gateway with potential for >6 degree northward migration of the STFZ during MIS 24, 936 – 917 ka and glacials after 900 ka are characterized by greater abundance of polar foraminifera and a reduced SST gradient between Sites U1475 and 1090, consistent with a more northern STFZ. More similar $\delta^{15}N_{FB}$ values between *G. bulloides* and *G. inflata* after MIS 24 also support a northern expansion of Southern Ocean nitrate and reduced influence of low $\delta^{15}N$ subtropical nitrate at Site U1475 after 900 ka. These data suggest that not only cooling of the Southern Ocean but also its expansion is necessary to expand the length of ice ages across the MPT.

The increases in $\delta^{15}N_{FB}$ associated with northward migrations of the front are likely amplified by changes in nutrient consumption. Despite higher supply of nitrate and reduced subtropical water contribution in MPT glacials, it seems that nutrient consumption increased, likely related to iron fertilization. Glacial expansion of the Southern Ocean has the potential to enlarge the total nutrient replete area and it also may facilitate iron fertilization by bringing these nutrient rich waters closer to Southern Hemisphere iron sources which would otherwise be unavailable. In this region, a >6 degree northward migration of the STFZ would deliver nitrate bearing surface waters into latitudes receiving twice as much annual dust deposition, linking physical and biological carbon feedbacks (Figure 1; Jaccard et al., 2016). A complimentary iron accumulation record from Site U1475 would allow us to determine whether northward expansion of the STFZ, and associated proximity to South African iron sources, could stimulate additional nutrient drawdown. A $\delta^{15}N_{FB}$ record from a site north of Site U1475 would allow us to account for any reduction of the $\delta^{15}N_{FB}$ values at Site U1475 due to mixing with subtropical water or changes in the proportion of fixation derived N.

A northward shift in the position of the STFZ in this region would alter physical ocean circulation, increasing the residence time of this carbon in the deep ocean. We hope that future work to generate nutrient consumption and Fe records will clarify the extent to which Fe fertilization further enhances C sequestration. This interplay between physical and biological feedbacks in the Indian-Atlantic Ocean Gateway may play a critical role in increasing deep ocean carbon storage and lengthening glacial cycles during the MPT.

Acknowledgments

Funding: Work was supported by NSF MGG award 1737218 and U.S. Science Support Program Post-Expedition Awards to R. S. R. and M. A. B.

Authors contributions: B. A. M., R. S. R., A. C-S. and M. A. B. conceived the project and contributed to the writing. B. A. M. and R. S. R. collected and analyzed the foraminifera bound N isotope data. T. P.d S. and D. L. collected and analyzed the foraminiferal assemblage data and

contributed to the interpretation and writing. I. A. H., A. S., and A. C-S. contributed to the data interpretation and writing.

Competing interests: The authors have no known competing interests at this time.

Open Research:

All new data presented in this paper are archived at Pangaea (Marcks et al., 2022a), (Marcks et al., 2022b), and (Marcks et al., 2022c).

References:

Altabet, M. A., & Francois, R. (1994). Sedimentary nitrogen isotopic ratio as a recorder for surface ocean nitrate utilization. *Global Biogeochemical Cycles*, *8*(1), 103–116. https://doi.org/10.1029/93GB03396

Anderson, R. F., Barker, S., Fleisher, M., Gersonde, R., Goldstein, S. L., Kuhn, G., Mortyn, P. G., Pahnke, K., & Sachs, J. P. (2014). Biological response to millennial variability of dust and nutrient supply in the Subantarctic South Atlantic Ocean. *Philosophical Transactions of the Royal Society A: Mathematical, Physical and Engineering Sciences*, *372*(2019), 20130054. https://doi.org/10.1098/rsta.2013.0054

Antell, G. S., Fenton, I. S., Valdes, P. J., & Saupe, E. E. (2021). Thermal niches of planktonic foraminifera are static throughout glacial–interglacial climate change. *Proceedings of the National Academy of Sciences*, *118*(18), e2017105118. https://doi.org/10.1073/pnas.2017105118

Bard, E., & Rickaby, R. E. M. (2009). Migration of the subtropical front as a modulator of glacial climate. *Nature*, *460*, 380-383. https://doi.org/10.1038/nature08189

Bé, A. W. H., Hutson, W. H., & Be, A. W. H. (1977). Ecology of Planktonic Foraminifera and Biogeographic Patterns of Life and Fossil Assemblages in the Indian Ocean. *Micropaleontology*, *23*(4), 369–369. https://doi.org/10.2307/1485406

Beal, L. M., De Ruijter, W. P. M., Biastoch, A., Zahn, R., Cronin, M., Hermes, J., Lutjeharms, J., Quartly, G., Tozuka, T., Baker-Yeboah, S., Bornman, T., Cipollini, P., Dijkstra, H., Hall, I., Park, W., Peeters, F., Penven, P., Ridderinkhof, H., & Zinke, J. (2011). On the role of the Agulhas system in ocean circulation and climate. *Nature*, *472*(7344), 429–436. https://doi.org/10.1038/nature09983

Becquey, S., & Gersonde, R. (2002). Past hydrographic and climatic changes in the Subantarctic Zone of the South Atlantic – The Pleistocene record from ODP Site 1090. *Palaeogeography, Palaeoclimatology, Palaeoecology*, *182*(3–4), 221–239. https://doi.org/10.1016/S0031-0182(01)00497-7

Beltran, C., Golledge, N. R., Christian, O., Kowalewski, D. E., Marie-Alexandrine, S., Hageman, K. J., Robert, S., Wilson, G. S., & François, M. (2020). Southern Ocean temperature records and

ice-sheet models demonstrate rapid Antarctic ice sheet retreat under low atmospheric CO2 during Marine Isotope Stage 31. *Quaternary Science Reviews*, *228*. https://doi.org/10.1016/j.quascirev.2019.106069

Bereiter, B., Eggleston, S., Schmitt, J., Nehrbass-Ahles, C., Stocker, T. F., Fischer, H., Kipfstuhl, S., & Chappellaz, J. (2015). Revision of the EPICA Dome C CO_2 record from 800 to 600 kyr before present: Analytical bias in the EDC CO2 record. *Geophysical Research Letters*, *42*(2), 542–549. https://doi.org/10.1002/2014GL061957

Billups, K., York, K., & Bradtmiller, L. I. (2018). Water Column Stratification in the Antarctic Zone of the Southern Ocean During the Mid-Pleistocene Climate Transition. *Paleoceanography and Paleoclimatology*, *33*(5), 432–442. https://doi.org/10.1029/2018PA003327

Braman RS, Hendrix SA. Nanogram nitrite and nitrate determination in environmental and biological materials by vanadium (III) reduction with chemiluminescence detection. Anal Chem. 1989 Dec 15;61(24):2715-8. doi: 10.1021/ac00199a007. PMID: 2619057.

Caley, T., Giraudeau, J., Malaizé, B., Rossignol, L., & Pierre, C. (2012). Agulhas leakage as a key process in the modes of Quaternary climate changes. *Proceedings of the National Academy of Sciences of the United States of America*, *109*(18), 6835–6839. https://doi.org/10.1073/pnas.1115545109

Cartagena-Sierra, A., Berke, M. A., Robinson, R. S., Marcks, B., Castañeda, I. S., Starr, A., Hall, I. R., Hemming, S. R., & LeVay, L. J. (2021). Latitudinal Migrations of the Subtropical Front at the Agulhas Plateau Through the Mid-Pleistocene Transition. *Paleoceanography and Paleoclimatology*, *36*(7), e2020PA004084. https://doi.org/10.1029/2020PA004084

Casciotti, K. L., Sigman, D. M., Hastings, M. G., Böhlke, J. K., & Hilkert, A. (2002). Measurement of the oxygen isotopic composition of nitrate in seawater and freshwater using the denitrifier method. Analytical chemistry, 74(19), 4905-4912. https://doi.org/10.1021/ac020113w

Chalk, T. B., Hain, M. P., Foster, G. L., Rohling, E. J., Sexton, P. F., Badger, M. P. S., Cherry, S. G., Hasenfratz, A. P., Haug, G. H., Jaccard, S. L., Martínez-García, A., Pälike, H., Pancost, R. D., & Wilson, P. A. (2017). Causes of ice age intensification across the mid-pleistocene transition. *Proceedings of the National Academy of Sciences of the United States of America*, *114*(50), 13114–13119. https://doi.org/10.1073/pnas.1702143114

Crundwell, M., Scott, G., Naish, T., & Carter, L. (2008). Glacial-interglacial ocean climate variability from planktonic foraminifera during the Mid-Pleistocene transition in the temperate Southwest Pacific, ODP Site 1123. *Palaeogeography, Palaeoclimatology, Palaeoecology*, *260*(1–2), 202–229. https://doi.org/10.1016/j.palaeo.2007.08.023

Diekmann, B., & Kuhn, G. (2002). Sedimentary record of the mid-Pleistocene climate transition in the southeastern South Atlantic (ODP Site 1090). *Palaeogeography, Palaeoclimatology, Palaeoecology*, *182*(3–4), 241–258. https://doi.org/10.1016/S0031-0182(01)00498-9

DiFiore, P. J., Sigman, D. M., Karsh, K. L., Trull, T. W., Dunbar, R. B., & Robinson, R. S. (2010). Poleward decrease in the isotope effect of nitrate assimilation across the Southern Ocean. Geophysical Research Letters, 37(17). https://doi.org/10.1029/2010GL044090

Dupuy, C., Pagano, M., Got, P., Domaizon, I., Chappuis, A., Marchesseau, G. and Bouvy, M. (2016) Trophic relationships between metazooplankton communities and their plankton food sources in the Iles Eparses (Western Indian Ocean). Marine Environmental Research 116, 18-31.

Farmer, J. R., Hönisch, B., Haynes, L. L., Kroon, D., Jung, S., Ford, H. L., Raymo, M. E., Jaume-Seguí, M., Bell, D. B., Goldstein, S. L., Pena, L. D., Yehudai, M., & Kim, J. (2019). Deep Atlantic Ocean carbon storage and the rise of 100,000-year glacial cycles. *Nature Geoscience*, 1–1. https://doi.org/10.1038/s41561-019-0334-6

Ferrari, R., Jansen, M. F., Adkins, J. F., Burke, A., Stewart, A. L., & Thompson, A. F. (2014). Antarctic sea ice control on ocean circulation in present and glacial climates. *Proceedings of the National Academy of Sciences of the United States of America*, *111*(24), 8753–8758. https://doi.org/10.1073/pnas.1323922111

Ford, B. H. L., & Chalk, T. B. (2020). THE MID-PLEISTOCENE ENIGMA. *Oceanography*, *33*(2), 101–103.

Fripiat, F., Martínez-García, A., Fawcett, S. E., Kemeny, P. C., Studer, A. S., Smart, S. M., Rubach, F., Oleynik, S., Sigman, D. M., & Haug, G. H. (2019). The isotope effect of nitrate assimilation in the Antarctic Zone: Improved estimates and paleoceanographic implications. *Geochimica et Cosmochimica Acta*, *247*, 261–279. https://doi.org/10.1016/j.gca.2018.12.003

Garcia, H. E., R. A. Locarnini, T. P. Boyer, J. I. Antonov, O.K. Baranova, M.M. Zweng, J.R. Reagan, D.R. Johnson, 2014. World Ocean Atlas 2013, Volume 4: Dissolved Inorganic Nutrients (phosphate, nitrate, silicate). S. Levitus, Ed., A. Mishonov Technical Ed.; NOAA Atlas NESDIS 76, 25 pp.

Gonfiantini, R., Stichler, W., & Rozanski, K. (1995). Standards and intercomparison materials distributed by the International Atomic Energy Agency for stable isotope measurements (No. IAEA-TECDOC--825).

Haddam, N. A., Michel, E., Siani, G., Cortese, G., Bostock, H. C., Duprat, J. M., & Isguder, G. (2016). Improving past sea surface temperature reconstructions from the Southern Hemisphere oceans using planktonic foraminiferal census data. *Paleoceanography*, *31*(6), 822–837. https://doi.org/10.1002/2016PA002946

Harms, N. C., Lahajnar, N., Gaye, B., Rixen, T., Dähnke, K., Ankele, M., Schwarz-Schampera, U., & Emeis, K.-C. (2019). *Nutrient distribution and nitrogen and oxygen isotopic composition of nitrate in water masses of the subtropical South Indian Ocean*. https://doi.org/10.5194/bg-2018511

Hasenfratz, A. P., Jaccard, S. L., Martínez-García, A., Sigman, D. M., Hodell, D. A., Vance, D., Bernasconi, S. M., Kleiven, H. F., Haumann, F. A., & Haug, G. H. (2019). The residence time of Southern Ocean surface waters and the 100,000-year ice age cycle. *Science*, 1080–1084. https://doi.org/10.1126/science.aat7067

Hönisch, B., Hemming, N., Archer, D., Siddall, M., & McManus, J. (2009). Atmospheric Carbon Dioxide Concentration Across the Mid-Pleistocene Transition. *Science (New York, N.Y.)*, *324*, 1551–1554. https://doi.org/10.1126/science.1171477

Hoogakker, B. A. A., Rohling, E. J., Palmer, M. R., Tyrrell, T., & Rothwell, R. G. (2006). Underlying causes for long-term global ocean δ13C fluctuations over the last 1.20 Myr. *Earth and Planetary Science Letters*, *248*(1–2), 15–29. https://doi.org/10.1016/j.epsl.2006.05.007

Jaccard, S. L., Hayes, C. T., Martínez-García, A., Hodell, D. A., Anderson, R. F., Sigman, D. M., & Haug, G. H. (2013). Two Modes of Change in Southern Ocean Productivity Over the Past Million Years. *Science*, *339*(6126), 1419–1423. https://doi.org/10.1126/SCIENCE.1227545

Jonkers, L., & Kučera, M. (2015). Global analysis of seasonality in the shell flux of extant planktonic Foraminifera. Biogeosciences, 12(7), 2207-2226. https://doi.org/10.5194/bg-12-2207-2015

Kaiser, E. A., Billups, K., & Bradtmiller, L. (2021). A 1 Million Year Record of Biogenic Silica in the Indian Ocean Sector of the Southern Ocean: Regional Versus Global Forcing of Primary Productivity. *Paleoceanography and Paleoclimatology*, *36*(3), e2020PA004033. https://doi.org/10.1029/2020PA004033

Kemp, A. E. S., Grigorov, I., Pearce, R. B., & Naveira Garabato, A. C. (2010). Migration of the Antarctic Polar Front through the mid-Pleistocene transition: Evidence and climatic implications. *Quaternary Science Reviews*, *29*(17–18), 1993–2009. https://doi.org/10.1016/j.quascirev.2010.04.027

Kennett, J.P., Srinivasan, M. (1983). Neogene Planktonic Foraminifera: A Phylogenetic Atlas. Hutchinson Ross, Stroudsburg (273 pp).

Khatiwala, S., Schmittner, A., & Muglia, J. (2019). Air-sea disequilibrium enhances ocean carbon storage during glacial periods. *Science Advances*, *5*(6), eaaw4981–eaaw4981. https://doi.org/10.1126/sciadv.aaw4981

Kim, J. E., Khim, B. K., Ikehara, M., & Lee, J. (2018). Orbital-scale denitrification changes in the Eastern Arabian Sea during the last 800 kyrs. Scientific Reports, 8(1), 1-8. https://doi.org/10.1016/j.margen.2021.100849

King, A. L., & Howard, W. R. (2003). Planktonic foraminiferal flux seasonality in Subantarctic sediment traps: A test for paleoclimate reconstructions. Paleoceanography, 18(1). https://doi.org/10.1029/2002PA000839

Knapp, A. N., Sigman, D. M., and Lipschultz, F. (2005), N isotopic composition of dissolved organic nitrogen and nitrate at the Bermuda Atlantic Time-series Study site, Global Biogeochem. Cycles, 19, GB1018, doi:10.1029/2004GB002320.

Kolasinski, J., Kaehler, S. and Jaquemet, S. (2012) Distribution and sources of particulate organic matter in a mesoscale eddy dipole in the Mozambique Channel (south-western Indian Ocean): Insight from C and N stable isotopes. Journal of Marine Systems 96-97, 122-131.

Kretschmer, K., Jonkers, L., Kucera, M., & Schulz, M. (2018). Modeling seasonal and vertical habitats of planktonic foraminifera on a global scale. Biogeosciences, 15(14), 4405-4429. https://doi.org/10.5194/bg-15-4405-2018

Laskar, J., Robutel, P., Joutel, F., Gastineau, M., Correia, A. C. M., & Levrard, B. (2004). A long-term numerical solution for the insolation quantities of the Earth. Astronomy & Astrophysics, 428(1), 261-285.

Lear, C. H., Billups, K., Rickaby, R. E. M., Diester-Haass, L., Mawbey, E. M., & Sosdian, S. M. (2016). Breathing more deeply: Deep ocean carbon storage during the mid-Pleistocene climate transition. *GEOLOGY*, *44*. https://doi.org/10.1130/G38636.1

Li, F., Ginoux, P., & Ramaswamy, V. (2008). Distribution, transport, and deposition of mineral dust in the Southern Ocean and Antarctica: Contribution of major sources. *Journal of Geophysical Research: Atmospheres*, *113*(D10). https://doi.org/10.1029/2007JD009190

Lisiecki, L. E. (2010). Links between eccentricity forcing and the 100,000-year glacial cycle. *Nature Geoscience*, *3*(5), 349–352. https://doi.org/10.1038/ngeo828

Loeblich, A., Tappan, H., 1988. Foraminiferal Genera and Their Classification. 2. van Nostrand Reinhold Company Publisher, pp. 1–212.

Maiorano, P., Marino, M., & Flores, J.-A. (2009). The warm interglacial Marine Isotope Stage 31: Evidences from the calcareous nannofossil assemblages at Site 1090 (Southern Ocean). *Marine Micropaleontology*, *71*(3–4), 166–175. https://doi.org/10.1016/j.marmicro.2009.03.002

Marcks, Basia; Santos, Thiago Pereira dos; Lessa, Douglas Villela de Oliveira; Cartagena-Sierra, Alejandra; Berke, Melissa A; Starr, Aidan; Hall, Ian R; Kelly, Roger P; Robinson, Rebecca S

(2022a): $\delta^{15}N$ in planktonic foraminifera species G. bulloides and G. inflata from IODP Site 361-U1475. [Dataset], PANGAEA, https://doi.org/10.1594/PANGAEA.945839

Marcks, Basia; Santos, Thiago Pereira dos; Lessa, Douglas Villela de Oliveira; Cartagena-Sierra, Alejandra; Berke, Melissa A; Starr, Aidan; Hall, Ian R; Kelly, Roger P; Robinson, Rebecca S (2022b): Abundance of Neogloboquadrina pachyderma sinistral from IODP Site 361-U1475. [Dataset], PANGAEA, https://doi.org/10.1594/PANGAEA.945840

Marcks, Basia; Santos, Thiago Pereira dos; Lessa, Douglas Villela de Oliveira; Cartagena-Sierra, Alejandra; Berke, Melissa A; Starr, Aidan; Hall, Ian R; Kelly, Roger P; Robinson, Rebecca S (2022c): Opal mass accumulation rates from IODP Site 361-U1475. [Dataset], PANGAEA, https://doi.org/10.1594/PANGAEA.945841

Marshall, J., & Speer, K. (2012). Closure of the meridional overturning circulation through Southern Ocean upwelling. Nature Geoscience, 5(3), 171-180.

Martin, J. H. (1990). Glacial-interglacial CO2 change: The Iron Hypothesis. *Paleoceanography*, *5*(1), 1–13. https://doi.org/10.1029/PA005i001p00001

Martínez-García, A., Rosell-Melé, A., Geibert, W., Gersonde, R., Masqué, P., Gaspari, V., & Barbante, C. (2009). Links between iron supply, marine productivity, sea surface temperature, and CO 2 over the last 1.1 Ma. *Paleoceanography*, *24*(1). https://doi.org/10.1029/2008PA001657

Martínez-García, A., Rosell-Melé, A., Jaccard, S. L., Geibert, W., Sigman, D. M., & Haug, G. H. (2011). Southern Ocean dust-climate coupling over the past four million years. *Nature*, *476*(7360), 312–315. https://doi.org/10.1038/nature10310

Martínez-García, A., Rosell-Mele, A., McClymont, E. L., Gersonde, R., & Haug, G. H. (2010). Subpolar Link to the Emergence of the Modern Equatorial Pacific Cold Tongue. *Science*, *328*(5985), 1550–1553. https://doi.org/10.1126/science.1184480

Martínez-García, A., Sigman, D. M., Ren, H., Anderson, R. F., Straub, M., Hodell, D. A., Jaccard, S. L., Eglinton, T. I., & Haug, G. H. (2014). Iron fertilization of the subantarctic ocean during the last ice age. *Science*, *343*(6177), 1347–1350. https://doi.org/10.1126/science.1246848

McKay, R., Naish, T., Carter, L., Riesselman, C., Dunbar, R., Sjunneskog, C., Winter, D., Sangiorgi, F., Warren, C., Pagani, M., Schouten, S., Willmott, V., Levy, R., DeConto, R., & Powell, R. D. (2012). Antarctic and Southern Ocean influences on Late Pliocene global cooling. *Proceedings of the National Academy of Sciences*, *109*(17), 6423–6428. https://doi.org/10.1073/pnas.1112248109

Monterey, G. I., & Levitus, S. (1997). Climatological cycle of mixed layer depth in the world ocean, report, 5 pp., NOAA, Silver Spring, Md. In NOAA Atlas NESDIS 14, Silver spring. Md: National Oceanic and Atmospheric Administration.

Mortlock, R. A., & Froelich, P. N. (1989). A simple method for the rapid determination of biogenic opal in pelagic marine sediments. Deep Sea Research Part A. Oceanographic Research Papers, 36(9), 1415-1426. https://doi.org/10.1016/0198-0149(89)90092-7

Muglia, J., Skinner, L. C., & Schmittner, A. (2018). Weak overturning circulation and high Southern Ocean nutrient utilization maximized glacial ocean carbon. *Earth and Planetary Science Letters*, *496*, 47–56. https://doi.org/10.1016/J.EPSL.2018.05.038

Nydahl & Folke (1978) On the peroxodisulfate oxidation of total nitrogen in waters to nitrate: Water Research, v. 12, p. 1123–1130. https://doi.org/10.1016/0043-1354(78)90060-X

Olbers, D., Gouretsky, V., Seiß, G., & Schröter, J. (1992). Hydrographic Atlas of the Southern Ocean. In *Alfred-Wegener-Institut, Bremerhaven*. https://epic.awi.de/id/eprint/2325/

Orsi, A. H., Whitworth, T., & Nowlin, W. D. (1995). On the meridional extent and fronts of the Antarctic Circumpolar Current. *Deep Sea Research Part I: Oceanographic Research Papers*, *42*(5), 641–673. https://doi.org/10.1016/0967-0637(95)00021-W

Peeters, F. J. C., Acheson, R., Brummer, G. J. A., De Ruijter, W. P. M., Schneider, R. R., Ganssen, G. M., Ufkes, E., & Kroon, D. (2004). Vigorous exchange between the Indian and Atlantic oceans at the end of the past five glacial periods. *Nature*, *430*(7000), 661–665. https://doi.org/10.1038/nature02785

Pena, L. D., & Goldstein, S. L. (2014). *Thermohaline circulation crisis and impacts during the mid-Pleistocene transition*. *Science* 345.6194 (2014): 318-322. https://doi.org/10.1126/science.1249770

Ren, H., Sigman, D. M., Meckler, A. N., Plessen, B., Robinson, R. S., Rosenthal, Y., & Haug, G. H. (2009). Foraminiferal isotope evidence of reduced nitrogen fixation in the ice age Atlantic ocean. *Science*, *323*(5911), 244–248. https://doi.org/10.1126/science.1165787

Robinson, R., Sigman, D., Difiore, P., Rohde, M., Mashiotta, T., Lea, D., & Robinson, C. (2005). Diatom-bound 15N/14N: New support for enhanced nutrient consumption in the ice age Subantarctic. *Paleoceanography*, *20*. https://doi.org/10.1029/2004PA001114

Robinson, R. S., Jones, C. A., Kelly, R. P., Rafter, P., Etourneau, J., & Martinez, P. (2019). A cool, nutrient-enriched eastern equatorial Pacific during the mid-Pleistocene transition. Geophysical Research Letters, 46(4), 2187-2195. https://doi.org/10.1029/2018GL081315

RStudio Team (2020). RStudio: Integrated Development for R. RStudio, PBC, Boston, MA URL http://www.rstudio.com/.

Russell, J. L., Dixon, K. W., Gnanadesikan, A., Stouffer, R. J., & Toggweiler, J. R. (2006). The Southern Hemisphere westerlies in a warming world: Propping open the door to the deep ocean. Journal of Climate, 19(24), 6382-6390.

Sigman, D. M., Altabet, M. A., Francois, R., McCorkle, D. C., & Gaillard, J.-F. (1999). The isotopic composition of diatom-bound nitrogen in Southern Ocean sediments. *Paleoceanography*, *14*(2), 118–134. https://doi.org/10.1029/1998PA900018

Sigman,D. M., Casciotti, K. L., Andreani, M., Barford, C., Galanter, M., and Böhlke, J. K., (2001). A Bacterial Method for the Nitrogen Isotopic Analysis of Nitrate in Seawater and Freshwater. *Analytical Chemistry*, 73(17), 4145-4153. DOI: 10.1021/ac010088e

Sigman, D. M., Hain, M. P., & Haug, G. H. (2010). The polar ocean and glacial cycles in atmospheric CO2 concentration. *Nature*, *466*(7302), 47–55. https://doi.org/10.1038/nature09149

Sigman, D. M., Fripiat, F., Studer, A. S., Kemeny, P. C., Martínez-García, A., Hain, M. P., ... & Haug, G. H. (2021). The Southern Ocean during the ice ages: A review of the Antarctic surface isolation hypothesis, with comparison to the North Pacific. Quaternary Science Reviews, 254, 106732.

Simon, M. H., Arthur, K. L., Hall, I. R., Peeters, F. J. C., Loveday, B. R., Barker, S., Ziegler, M., & Zahn, R. (2013). Millennial-scale Agulhas Current variability and its implications for saltleakage through the Indian-Atlantic Ocean Gateway. *Earth and Planetary Science Letters*, *383*, 101–112. https://doi.org/10.1016/j.epsl.2013.09.035

Smart, S. M., Fawcett, S. E., Ren, H., Schiebel, R., Tompkins, E. M., Martínez-García, A., Stirnimann, L., Roychoudhury, A., Haug, G. H., & Sigman, D. M. (2020). The nitrogen isotopic composition of tissue and shell-bound organic matter of planktic foraminifera in Southern Ocean surface waters. *Geochemistry, Geophysics, Geosystems*, *21*(2). https://doi.org/10.1029/2019gc008440

Starr, A., Hall, I. R., Barker, S., Rackow, T., Zhang, X., Hemming, S. R., van der Lubbe, H. J. L., Knorr, G., Berke, M. A., Bigg, G. R., Cartagena-Sierra, A., Jiménez-Espejo, F. J., Gong, X., Gruetzner, J., Lathika, N., LeVay, L. J., Robinson, R. S., Ziegler, M., Brentegani, L., … Zhang, H. (2021). Antarctic icebergs reorganize ocean circulation during Pleistocene glacials. *Nature*, *589*(7841), 236–241. https://doi.org/10.1038/s41586-020-03094-7

Tangunan, D., M. A. Berke, A. Cartagena-Sierra, J. A. Flores, J. Gruetzner, F. Jiménez-Espejo, L. J. LeVay, K.-H. Baumann, O. Romero, and M. Saavedra-Pellitero (2021), Strong glacial-interglacial variability in upper ocean hydrodynamics, biogeochemistry, and productivity in the southern Indian Ocean, Communications Earth & Environment, 2(1), 1-13. https://doi.org/10.1038/s43247-021-00148-0

Toggweiler, J. R., Russell, J. L., & Carson, S. R. (2006). Midlatitude westerlies, atmospheric CO2, and climate change during the ice ages. Paleoceanography, 21(2).

van Sebille, E., Scussolini, P., Durgadoo, J. V., Peeters, F. J., Biastoch, A., Weijer, W., ... & Zahn, R. (2015). Ocean currents generate large footprints in marine palaeoclimate proxies. Nature communications, 6(1), 1-8. https://doi.org/10.1038/ncomms7521

Wang, P., Tian, J., Cheng, X., Liu, C., & Xu, J. (2004). Major Pleistocene stages in a carbon perspective: The South China Sea record and its global comparison. *Paleoceanography*, *19*(4), n/a-n/a. https://doi.org/10.1029/2003PA000991

Yang, H., Lohmann, G., Krebs-Kanzow, U., Ionita, M., Shi, X., Sidorenko, D., Gong, X., Chen, X., & Gowan, E. J. (2020). Poleward Shift of the Major Ocean Gyres Detected in a Warming Climate. *Geophysical Research Letters*, *47*(5), e2019GL085868. https://doi.org/10.1029/2019GL085868

Zahn, R. (2009). Beyond the CO2 connection. *Nature*, *460*(7253), 335–336. https://doi.org/10.1038/46

935